

1  
2  
3  
4  
5  
6  
7  
8  
9  
10  
11  
12  
13  
14  
15  
16  
17  
18  
19  
20  
21  
22  
23  
24  
25  
26  
27  
28  
29  
30  
31

Article type : Research Article

**Exomer complex regulates protein traffic at the TGN through differential interactions with cargos and clathrin adaptor complexes**

Running title: Exomer and the recycling of transmembrane proteins.

Carlos Anton-Plagaro<sup>1,2\*</sup>, Noelia Sanchez<sup>1</sup>, Rosario Valle<sup>1</sup>, Jose Miguel Mulet<sup>3</sup>, Mara C. Duncan<sup>4</sup> and Cesar Roncero<sup>1\*</sup>

<sup>1</sup>Instituto de Biología Funcional y Genómica (IBFG) and Departamento de Microbiología y Genética, CSIC-Universidad de Salamanca, Salamanca, Spain; <sup>2</sup>Present address: School of Biochemistry, University of Bristol, Bristol, UK; <sup>3</sup>Instituto de Biología Molecular y Celular de Plantas, CSIC-Universitat Politècnica de València, Valencia, Spain; <sup>4</sup>Cell and Developmental Biology Department, University of Michigan, Ann Arbor, MI, USA.

\*Corresponding authors:

- Dr. Carlos Anton-Plagaro  
Biomedical Sciences Building (University of Bristol)  
Tankard's Cl, University Walk, Bristol BS8 1TD, UK  
E-mail: carlos.antonplagaro@bristol.ac.uk

- Prof. Cesar Roncero

This is the author manuscript accepted for publication and has undergone full peer review but has not been through the copyediting, typesetting, pagination and proofreading process, which may lead to differences between this version and the [Version of Record](#). Please cite this article as [doi: 10.1002/FSB2.21615](https://doi.org/10.1002/FSB2.21615)

This article is protected by copyright. All rights reserved

32 IBFG  
33 C/ Zacarías González  
34 37007, Salamanca, Spain  
35 E-mail: crm@usal.es  
36 Phone: 34-923-294883 FAX: 34-923-224876

37

38

39 **ABBREVIATIONS**

40

41 TGN: *trans* Golgi network

42 PM: plasma membrane

43 PVC: pre-vacuolar compartment

44 EE: early endosomes

45 MVB: multi vesicular body

46 ER: Endoplasmic reticulum

47 BIFC: Bimolecular fluorescence complementation

48 CCV: clathrin coated vesicles

49 AP-1: clathrin adaptor complex-1

50 GGA: Golgi-localizing, Gamma-adaptin ear homology, ARF-binding proteins

51 PtdIns(4)P: Phosphatidylinositol 4-phosphate

52 ChAP: Chs5-Arf1 binding proteins

53 PCR: polymerase chain reaction

54 ORF: open reading frame

55 GFP: green fluorescent protein

56 HA: Human influenza hemagglutinin epitope

57 YEP: yeast extract and peptone medium

58 YEPD: yeast extract, peptone and dextrose medium

59 SD: synthetic defined medium

60 YNB-N-aa: yeast nitrogen base without nitrogen and without amino acids

61 CW: calcofluor white

62 IC50: half maximal inhibitory concentration

63 OD<sub>600</sub>: optical density at wavelength of 600nm

64 TCA: trichloroacetic acid

65 DTT: dithiothreitol

66 SDS: sodium dodecyl sulfate  
67 BSA: bovine serum albumin  
68 RT: room temperature  
69 O/N: overnight  
70 3-AT: 3-aminotriazole  
71 AzC: L-azetidin-2-carboxilate  
72 AAP: amino acid permease  
73 SPS: Ssy1p-Ptr3p-Ssy5 cellular sensor  
74 NCR: Nitrogen Catabolite Repression  
75 TORC1: target of rapamycin kinase complex I  
76 GEF: guanine nucleotide exchange factor  
77 GAP: GTPase activating protein  
78 mR2: mRuby2 epitope  
79 VC: C terminus fragment of Venus fluorescent protein  
80 VN: N terminus fragment of Venus fluorescent protein  
81 ROI: Region of interest

82  
83  
84

## ABSTRACT

85  
86 Protein sorting at the *trans* Golgi network (TGN) usually requires the assistance  
87 of cargo adaptors. However, it remains to be examined how the same complex can  
88 mediate both the export and retention of different proteins or how sorting complexes  
89 interact among themselves. In *Saccharomyces cerevisiae*, the exomer complex is  
90 involved in the polarized transport of some proteins from the TGN to the plasma  
91 membrane (PM). Intriguingly, exomer and its cargos also show a sort of functional  
92 relationship with TGN clathrin adaptors that is still unsolved. Here, using a wide range  
93 of techniques, including time-lapse and BIFC microscopy, we describe new molecular  
94 implications of the exomer complex in protein sorting and address its different layers of  
95 functional interaction with clathrin adaptor complexes. Exomer mutants show impaired  
96 amino acid uptake because it facilitates not only the polarized delivery of amino acid  
97 permeases to the PM but also participates in their endosomal traffic. We propose a  
98 model for exomer where it modulates the recruitment of TGN clathrin adaptors directly  
99 or indirectly through Arf1 function. Moreover, we describe an *in vivo* competitive

100 relationship between the exomer and AP-1 complexes for the model cargo Chs3. These  
101 results highlight a broad role for exomer in regulating protein sorting at the TGN that is  
102 complementary to its role as cargo adaptor and present a model to understand the  
103 complexity of TGN protein sorting.

## 106 INTRODUCTION

108 The trans Golgi network (TGN) is a major intracellular cargo sorting station,  
109 where newly synthesized proteins and endocytosed proteins need to be accurately  
110 identified and sorted to distinct subcellular destinations (1). Cells utilize sophisticated  
111 cargo sorting machineries to meticulously package the cargo molecules into the right  
112 transport carriers (1). During this process, cargo adaptors often play pivotal roles in both  
113 cargo recognition and in coat assembly (2, 3), while coat assembly ultimately leads to  
114 membrane deformation and fission (4). One critical coat at the TGN is the clathrin coat,  
115 which generates clathrin-coated vesicles (CCV). Although it is clear that in most  
116 eukaryotes the clathrin adaptor complex-1 (AP-1) plays a critical role in TGN sorting,  
117 growing evidence suggests it may play a role in both export and retention, moreover  
118 AP-1 shows genetic interaction with several other sorting complexes suggesting  
119 communication between complexes may help maintain the protein sorting function (2,  
120 3). CCV assembly has been extensively analyzed in the yeast *Saccharomyces cerevisiae*  
121 (5). In this yeast, several clathrin adaptors are sequentially recruited to TGN membranes  
122 through a coordinated mechanism that depends on PtdIns(4)P and the Arf1 GTPase (3).  
123 The adaptor complex GGA is first recruited, followed by AP-1. Deletion of Gga2 alters  
124 the dynamics of the recruitment of AP-1. By contrast, AP-1 has minor mechanistic  
125 effects in the assembly of the other clathrin adaptor complexes (6). Clathrin and its  
126 adaptor complexes have a general role in the regulation of the traffic of multiple  
127 proteins to the pre-vacuolar compartment (PVC) facilitating their recycling back to the  
128 TGN. Accordingly, the involvement of these complexes in the late endosomal traffic of  
129 multiple amino acid transporters has been described (7-10). Recycling from the PVC  
130 has been well characterized for TGN resident proteins like Kex2, Vps10 and Tlg1 (11-  
131 13). However, a role for clathrin in the formation of a distinct subset of secretory  
132 vesicles has also been reported (14), but the nature of these vesicles and their cargos has  
133 remained elusive.

134 The function of clathrin and its adaptors in the anterograde traffic from the TGN  
135 to PM is poorly understood, yet another sorting complex, exomer, has a more  
136 established role in this TGN to PM traffic. The exomer complex is a cargo adaptor  
137 required for the delivery of three cargoes to the PM, the major chitin synthase, Chs3,  
138 (15-17), Fus1 (18), and Pin2 (19), all three integral transmembrane proteins. Exomer  
139 consists of a tetramer formed by a dimer of the scaffold protein Chs5 and two accessory  
140 proteins (20) that are encoded by four different genes: the paralogous *BCH1 / BUD7*  
141 and *CHS6 / BCH2* gene pairs (17, 21). Together these four proteins are called the  
142 ChAPs (Chs5-Arf1 binding proteins). The ChAPs are thought to bind directly to cargoes,  
143 Arf1, and membranes thereby acting as the cargo recognition face of the complex. The  
144 current view is that any two of the four ChAPs can be incorporated into the exomer  
145 complexes, providing different functionalities (21-23). For example, only an exomer  
146 containing the Chs6 ChAP is able to mediate the traffic of Chs3 to the PM (17, 21, 24),  
147 because Chs3 interacts physically with the exomer through the Chs6 ChAP (24-26). In  
148 contrast, the Bch1 Bud7 paralogous proteins appear to interact directly with the TGN  
149 membrane to favor the membrane curvature required for vesicle formation (22).

150 Interestingly, all known exomer cargoes are also subject to AP-1-mediated traffic  
151 (18, 19, 27). This was first reported for Chs3, where deletion of the AP-1 complex  
152 restores Chs3 PM localization in cells lacking exomer (25, 27). This restoration is  
153 thought to indicate a role for clathrin and AP-1 in the retention of Chs3 at the TGN (27),  
154 which allows the exomer to deliver Chs3 to the PM in a cell cycle or stress-regulated  
155 manner (28). The mechanistic relationship between exomer and AP-1 complexes in this  
156 retention mechanism is unclear. In addition, exomer is well conserved in other fungi  
157 (21, 29), and it has been recently reported that the *Schizosaccharomyces pombe* exomer  
158 interacts functionally with clathrin adaptors as a means to maintain the integrity of  
159 diverse cellular compartments (30). Taken together, these results, reported in several  
160 organisms, highlight the potential multiple levels of interaction among exomer and  
161 other TGN complexes in order to facilitate protein traffic.

162 In this work, we explored additional roles for exomer in protein traffic and its  
163 unsolved relationship with TGN clathrin adaptors using multiple approaches. We show  
164 that exomer not only facilitates the anterograde traffic of several integral PM proteins  
165 from the TGN, but also plays a general role in protein traffic by modulating the  
166 assembly of TGN clathrin adaptors thus regulating proper traffic from the TGN to the

167 PVC. Finally, we conclude that exomer maintains different associations with cargos and  
168 clathrin adaptors, which differ along fungal lineage.

169

170

171

172

173

174

175

## 176 MATERIAL AND METHODS

### 177 Yeast strains construction.

178 The yeasts strains used throughout this work were made in the W303, BY4741  
179 or X2180 genetic backgrounds as indicated in the Table 1. Cells were transformed using  
180 lithium acetate/ polyethylene glycol procedure (31). Gene deletions were made using a  
181 PCR-mediated gene replacement technique, using different deletion cassettes based on  
182 the *natMX4*, *kanMX4*, or *hphNT1* resistance genes (32). For the insertion of the GAL1  
183 promoter in front of ORFs, the cassette was amplified from pFA6a-*kanMX4*::pGAL1  
184 (33) (Table 2). Proteins were tagged chromosomally at their C-terminus with 3xHA,  
185 GFP, mCherry and Venus CT or NT fragments, employing integrative cassettes  
186 amplified from pFA6a-3xHA::*hphMx6*/ pFA6a-GFP::*hphMx6*/ pFA6a-GFP::*natMx4*/  
187 pFN21/ pFA6a-VN::*HIS3Mx6*/ pFA6a-VC::*kanMX6* (34). The *Delitto Perfetto*  
188 technique was performed to generate the internal gene modifications within the genome.  
189 In brief, this approach allows for *in vivo* mutagenesis using two rounds of homologous  
190 recombination. The first step involves the insertion of a cassette containing two markers  
191 at or near the locus to be altered and the second involves complete removal of the  
192 cassette and transfer of the expected genetic modification to the chosen DNA locus as  
193 previously described (35).

194 *Construction of TAT2<sup>52-53</sup>-3xHA.* To obtain a fully functional tagged version of  
195 Tat2, we generated a chromosomally internally-tagged version of Tat2 in a region  
196 suitable for causing less reduced interference in Tat2 function, regulation and transport  
197 (between amino acids 52-53) using the *Delitto Perfetto* technique. Contrary to the GFP  
198 versions, this HA tagged protein fully complemented the *tat2Δ*-associated phenotypes,  
199 and importantly, had no effect on the *chs5Δ* requirement for external tryptophan. For  
200 microscopic localization we used a GFP C-terminus tagged version of the protein. This

201 protein is functional based on the complementation of the *tat2Δ* mutant, but showed a  
202 reduced rate of endocytosis (36).

203 The *C. albicans* mutants were generated as previously described (29).

204

### 205 **Media and growth assays.**

206 Yeast cells were grown at 28°C in YEPD (1 % Bacto yeast extract, 2 % peptone,  
207 2 % glucose), in SD medium (2 % glucose, 0.7 % Difco yeast nitrogen base without  
208 amino acids) or SD-N (2 % glucose, 0.16 % Difco yeast nitrogen base without  
209 ammonium and amino acids) supplemented with the pertinent amino acids and 2 % agar  
210 in the case of solid media. Calcofluor white (CW) sensitivity was always tested on  
211 YEPD or SD medium buffered with 50 mM potassium phthalate at pH 6.2 as described  
212 (37).

213 *C. albicans media.* LEE (2 % agar, 0.5 % (NH<sub>4</sub>)<sub>2</sub>SO<sub>4</sub>, 0.25 % K<sub>2</sub>HPO<sub>4</sub>, 0.02 %  
214 MgSO<sub>4</sub>·7H<sub>2</sub>O, 0.5 % NaCl, 0.05 % proline, 1.25 % glucose), LEE NAGA (LEE w/o  
215 glucose + 1.25 % N-Acetylglucosamine), LEE SERUM (LEE + 4 % fetal bovine  
216 serum) and M199 (M199 [Gibco BRL], 2 % agar, 80 mg/L uridine).

217 *Drop tests.* To assess the growth phenotypes, cells of each tested strain from  
218 early logarithmic cultures were resuspended in water and adjusted to an OD<sub>600</sub> of 1.0.  
219 Ten-fold serial dilutions were prepared and drops were spotted onto the appropriate agar  
220 plates containing media supplemented as indicated. Plates were incubated at 28°C for 2-  
221 5 days.

222 *Quantification of half maximal inhibitory concentration (IC50).* Sensitivity to  
223 myriocin and sertraline was analyzed in liquid YEPD media by growing strains in a 96-  
224 well plate with different drug concentrations and measuring the OD<sub>600</sub> using a Spectra  
225 Max 340PC plate reader as described in (38).

226

### 227 **Fluorescence microscopy.**

228 Yeast cells expressing GFP/ mCherry/ Venus tagged proteins were grown to  
229 early logarithmic phase in SD medium supplemented with 0.2 % adenine. Living cells  
230 were visualized directly by fluorescence microscopy. The bimolecular fluorescence  
231 complementation (BIFC) technique was used to analyze proximity among different  
232 proteins *in vivo* (39). For CW staining, 50 μg/ml CW was directly added to the fresh  
233 cells growing in YEPD and the cultures were incubated at 28°C for 1h before images  
234 were taken (40).

235 For non-quantitative purposes, images were routinely obtained using a Nikon  
236 90i Epifluorescence microscope (x100 objective; NA: 1.45) equipped with a  
237 Hamamatsu ORCA ER digital camera, specific Chroma filters (49000 ET-DAPI, 49002  
238 ET-GFP, 49003 ET-YFP, 49005 ET-DsRed) and controlled by *Metamorph* software.  
239 Images for quantitative purposes, such as co-localization, particle description or stream  
240 time-lapse of TGN-tagged proteins were acquired in a Spinning Disk confocal  
241 microscope (Olympus IX81 with Roper technology) with an Evolve EMCCD camera,  
242 100X/1.40 Plan Apo lens, 488nm / 561nm lasers, 525/45 - 609/54 Semrock emission  
243 filters and controlled by *Metamorph 7.7* software.

244

#### 245 **Protein extracts and immunoblotting.**

246 The trichloroacetic acid (TCA) protocol was used for protein processing for the  
247 Western blot analyses. Extracts were made using an equal numbers of cells from  
248 logarithmic growing cultures. Cells were centrifuged, resuspended in 20 % TCA, and  
249 frozen at -80°C for at least 3 hours. The samples were then thawed on ice and the  
250 centrifuged cells were disrupted in 1.5 ml tubes with 100 µl of 20 % TCA and glass  
251 beads (0.45 mm, SIGMA), during 3 pulses of 30 seconds with an intensity of 5.5 in a  
252 Fast prep (FP120, BIO101). Extracts were transferred to new tubes and 5% TCA was  
253 added to dilute TCA concentration to 10 %. Precipitated proteins were collected by  
254 centrifugation at 900xg for 10 min and the supernatant was completely discarded.  
255 Pelleted proteins were resuspended in 50 µl of 2x Sample Buffer (100 mM Tris-HCl pH  
256 6.8, 4 % SDS, 20 % glycerol, 25 mM DTT and traces of bromophenol blue) by  
257 vortexing, followed by the addition of 50µl of 2 M Tris-HCl pH 7.5. Samples were  
258 maintained on ice throughout this process. Finally, the extracts were heated to 37°C for  
259 30 min (for multipass transmembrane proteins) or 95°C for 5 min (for other proteins)  
260 and centrifuged for 5 min at 15000xg. The supernatant was collected and 15µl were  
261 used for Western blot analysis.

262 Extracts were separated on 7.5 % SDS-PAGE and transferred to PVDF  
263 membranes (37). The membranes were then blocked with TBST (Tris-buffered saline  
264 with 0.1% Tween 20) supplemented with 3 % non-fat dry milk for 1 hour and incubated  
265 with the corresponding antibodies in TBST with 3 % milk for 2 h at room temperature  
266 (RT) or overnight (O/N) at 4°C: anti-GFP JL-8 monoclonal antibody (Living colors,  
267 Clontech), anti-HA 12CA5 (Roche), anti-tubulin (T5162 Sigma). The blots were  
268 developed using anti-Rsp6-P (Cell SignalingTech: Phospho-Ser/Thr Akt Substrate



269 Antibody #9611s) and 5 % BSA replaced the non-fat dry milk in all steps. After 3  
270 washes with TBST, the membranes were incubated for 50 min together with the  
271 secondary antibodies in TBST with 3 % milk: polyclonal anti-Mouse or anti-Rabbit  
272 conjugated with horseradish peroxidase. After 3 washes with TBST, the blots were  
273 developed using the ECL kit (Advansta).

274

#### 275 **Subcellular fractionation by centrifugation in a sucrose gradient.**

276 For subcellular fractionations, 50 ml of culture with an OD<sub>600</sub> of 0.8-1 were  
277 collected and NaN<sub>3</sub> and NaF were added up to a final concentration of 20 mM. The  
278 cultures were centrifuged at 4°C at 4000xrpm for 4 min, resuspended with ice-cold  
279 water in 1.5 ml tubes, centrifuged at 6000xrpm for 2 min and resuspended in 1 ml of  
280 Azida Buffer (10 mM DTT, 20 mM NaN<sub>3</sub>, 20 mM NaF, 100 mM Tris-HCl pH 9.4).  
281 After a 10-minute incubation step at RT, the samples were centrifuged at 6000xrpm for  
282 2 min and resuspended in 600 µl of Spheroplast Buffer (1 M sorbitol, 20 mM NaN<sub>3</sub>, 20  
283 mM NaF, 10 mM Tris-HCl pH 7.5 in YEPD medium). Afterwards, 60 µl of zymolyase  
284 (100T, unfiltered, 4.76 mg/ml) were added and incubated at 30°C during 30-40 min  
285 under gentle mixing until spheroplasts were produced based on microscopic analysis.  
286 The spheroplast samples were then washed twice with spheroplast buffer and collected  
287 by 500xg centrifugation for 4 min at 4°C. The washed spheroplasts were incubated with  
288 300 µl Lysis Buffer (10 % sucrose, protease inhibitors, 1 mM PMSF, 1 mM EDTA, 20  
289 mM Tris-HCl pH 7.5) and incubated 10 min at RT with gradual pipetting (6-8 times).  
290 Lysis was microscopically assessed. Then, cell debris was removed by centrifugation at  
291 500xg for 4min at 4°C, the supernatants were collected and 250 µl of the supernatants  
292 were layered on the top of a mini-step sucrose gradient (EDTA 5 mM, 50 mM Tris-HCl  
293 pH7.5) made as follows: 300 µl 55%, 750 µl 45%, 500 µl 41%, 300 µl 37%, 250 µl  
294 29%. The gradients were centrifuged at 200,000xg for 3.5 h at 4°C (Beckman Coulter  
295 L-80 XP, SW 55 Ti rotor) and 7 fractions of 300 µl were manually collected from the  
296 top of the gradient. Finally, 100 µl of each fraction were denatured in the sample buffer  
297 plus 1 % SDS for 30 min at 37°C.

298

#### 299 **Tryptophan uptake assay.**

300 Tryptophan was measured adapting protocols previously described (36, 41).  
301 Specifically, cells were grown to early log phase in 50 mL of SD medium (without Trp)

302 at 30°C until an OD<sub>600</sub> of 0.4-0.8. Then, the cells were washed twice with wash buffer  
303 (10 mM sodium citrate, pH 4.5, and 20 mM (NH<sub>4</sub>)<sub>2</sub>SO<sub>4</sub>) and resuspended in 3.6 ml of  
304 incubation medium (10 mM sodium citrate, pH 4.5, 20 mM (NH<sub>4</sub>)<sub>2</sub>SO<sub>4</sub>, and 2 %  
305 glucose). The absorbance at 600 nm was measured to refer values to cell number. The  
306 assay was initiated by the addition of 400 µl of radiolabeled tryptophan solution (390 µl  
307 of the incubation medium and 10 µl of L-[5-<sup>3</sup>H]-tryptophan at 31 Ci/mmol GE  
308 healthcare, UK). Two aliquots (500 µl) were collected at each time point and chilled by  
309 the addition of 1 ml of the ice-cold incubation medium. Cells were collected by  
310 filtration through a nitrocellulose filter (0.45 µm pore size, 25 mm diameter [Millipore  
311 HAWP]) and washed three times with chilled water. Moist filters were transferred to  
312 Filter Count solution (Perkin Elmer, USA). Radioactivity was measured using a Tri-  
313 Carb® 4910 TR liquid scintillation counter (Perkin Elmer, USA).

314

#### 315 **Digital quantification, statistics and figure design.**

316 Microscopy and Western blot image processing and quantification were  
317 performed using *ImageJ-FIJI* software (1.48k version, NIH). For quantification of dot  
318 co-localization, pre-filtering with a custom built *ImageJ* Macro (Macro1, see Table 3)  
319 was followed by the analysis of the co-localization using the JACoP *ImageJ* plugin  
320 (co-localization based on centers of mass-particles coincidence, particle size 4-∞  
321 pixels). For the particle descriptors (intensity and area), ROIs were selected using a  
322 custom built Macro (Macro2, see Table 3), applying the same intensity threshold per  
323 experiment and loaded to ROIManager with AnalyzeParticles (0.07-∞ µm<sup>2</sup>, exclude on  
324 edges). In the case of Chs3-GFP TGN-EE structures, due to the difficulty of the  
325 segmentation, dots were selected manually for maximum intensity and maximum  
326 diameter quantification. A more detailed description of the macros used is presented in  
327 the supplementary materials.

328 For the quick time-lapse experiments, continuous images were acquired through  
329 the streaming mode on a Spinning Disk microscope in 3 z-planes separated by 0.2 µm  
330 to avoid loss of the highly dynamic TGN-structures in z-axis and to partially reduce  
331 photo-bleaching. Z-maximum intensity projections were analyzed manually or with the  
332 TrackMate *ImageJ* plugin. For the Sec7-mR2 structures, tracking was done using the  
333 TrackMate *ImageJ* plugin (LoG detector, Diameter 0.5 µm, Threshold 80, Median filter,  
334 Sub-pixel loc.; LAP Tracker; Frame to Frame 0.5 µm, No Gap, Split 0.5µM, Merge 0.5

335  $\mu\text{m}$ , tracks with  $\geq 5$  spots). The analysis was performed only on tracks that initiated and  
336 completed during the collection. For analyzing the recruitment of the exomer and  
337 clathrin adaptor complexes, images were taken of strains expressing *CHS5*-mCh/*GGAI*-  
338 GFP and *CHS5*-mCh/*APSI*-GFP. Afterwards, only the trajectories of structures  
339 showing both signals (mCh/GFP), present for  $\geq 10$  s, were selected manually or with the  
340 help of TrackMate (LoG detector, Diameter 1  $\mu\text{m}$ , Threshold 15-30, Median filter, Sub-  
341 pixel loc.; LAP Tracker; Frame to Frame 0.5  $\mu\text{m}$ , No Gap, No Split, No Merge,  
342 Duration  $\geq 8$ s) and the *Extract track stack* option (half of vesicles extracted from each  
343 channels). The average recruitment duration (temporal region with intensity  $\geq 25$  % of  
344 the maximum intensity per channel), as well as the temporal distance between  
345 maximum intensity peaks referring to Chs5-mCh for 30 trajectories, were manually  
346 calculated.

347 To obtain an unbiased measurement of the cellular polarization of PM proteins,  
348 the daughter/mother plasma membrane signal coefficient (polarization coefficient) of  
349 single cells was determined as described (42).

350 Image measurements were statistically analyzed using the T-test for unpaired  
351 data in *GraphPad Prism 6* software (GraphPad Software, Inc., La Jolla, USA).  
352 Significantly different values ( $P < 0.05$ ,  $P < 0.01$ ,  $P < 0.001$ ,  $P < 0.0001$ ) are indicated  
353 (\*, \*\*, \*\*\*, \*\*\*\*).

354 The presented images were prepared using *Adobe Photoshop CS5* and *Adobe*  
355 *Illustrator CS5* (San José, CA, USA) software. All images shown in each series were  
356 acquired under identical conditions and processed in parallel to preserve the relative  
357 intensities of fluorescence for comparative purposes. If not indicated, the scale bar  
358 represents 5  $\mu\text{m}$ .

359

## 360 RESULTS

361

362 **Exomer mutants show ammonium sensitivity due to the reduced uptake of**  
363 **tryptophan.** Exomer has been described to function as a cargo adaptor complex based  
364 on its role in the transport of Chs3, the catalytic subunit of the major chitin synthase in  
365 budding yeast (17, 21, 24). However, our recent work, based on the evolutionary  
366 characterization of exomer function across the fungi kingdom, suggests exomer may  
367 have additional functions (29). More importantly, *S. cerevisiae* exomer mutants showed

368 multiple phenotypes that cannot be explained by known cargoes of exomer such as  
369 sensitivity to ammonium (21, 29).

370 In an effort to better understand the functionality of exomer, we first confirmed  
371 the ammonium sensitivity of the exomer mutant *chs5Δ* by showing that this mutant  
372 grew poorly in YEPD supplemented with 0.2 M ammonium (Figure 1A). This  
373 sensitivity was also observed in SD media (Figure S1A). Interestingly, the absence of  
374 the two paralogous pairs of ChAPs produced different growth phenotypes (Figure 1A).  
375 The *bch1Δ bud7Δ* double mutant was as sensitive to ammonium as *chs5Δ*; however  
376 *chs6Δ bch2Δ* double mutant was not sensitive to ammonium. This result is notable since  
377 Chs6/Bch2 are known to function as cargo adaptors, whereas Bch1/Bud7 are thought to  
378 function in membrane association without cargo selectivity (22-24). These results could  
379 therefore reflect a role for exomer that is independent of its function as cargo adaptor.

380 A first indication for the source of the ammonium sensitivity of the exomer  
381 mutants came from the observation that the *chs5Δ* mutant was not sensitive to  
382 ammonium in the prototrophic X2180 background (Figure S1A). Although ammonium  
383 toxicity in yeast is poorly understood, one mechanism for ammonium detoxification  
384 involves the active excretion of amino acids across the PM (43). We hypothesized that  
385 as cells excrete amino acids as a response to ammonium toxicity, they deplete internal  
386 pools of amino acids and the prototrophic strain is able to compensate by synthesizing  
387 higher levels of the essential amino acids. We further pinpointed the key auxotrophic  
388 requirement through the observation that the *chs5Δ* mutant was not sensitive to  
389 ammonium in the BY strain, which differs from W303 in that it is not auxotrophic for  
390 tryptophan. In order to confirm this, we transformed the *chs5Δ* mutant in the W303  
391 background with different plasmids that restore the ability to synthesize amino acids for  
392 each auxotrophy. The restoration of the ability to synthesize tryptophan by a plasmid  
393 encoding *TRP1*, strongly reduced the ammonium sensitivity of the *chs5Δ* mutant, while  
394 the plasmid containing *HIS3* and *URA3* genes showed no effect on ammonium  
395 sensitivity (Figure S1B). By contrast, restoration of the ability to synthesize leucine by a  
396 plasmid encoding *LEU2* slightly reduced ammonium sensitivity. Moreover, the addition  
397 of tryptophan to the medium also abolished ammonium sensitivity in all strains. These  
398 results could indicate that the *chs5Δ* mutant has a reduced uptake of tryptophan, and,  
399 therefore, this mutant may require higher amounts of external tryptophan for growth.  
400 Consistent with this model, the wild-type auxotroph strain in SD media could form  
401 colonies with as little as 0.001 mg/ml of tryptophan, while the *chs5Δ* mutant required 8

402 times more tryptophan in the medium to obtain substantial colony growth (Figure 1B).  
403 In order to confirm these results, we measured tryptophan uptake directly (Figure 1C).  
404 Consistent with the increased requirement for extracellular tryptophan, tryptophan  
405 uptake was severely reduced in the absence of exomer compared to wild-type yeast.  
406 However, uptake was not as low as cells lacking the tryptophan permease Tat2 (44).  
407 Together these results show that in exomer mutants, the deficient uptake of tryptophan  
408 restricts the growth of tryptophan auxotrophs in a low concentration of tryptophan or in  
409 the presence of ammonium.

410

411 **Deficient Trp uptake of exomer mutants is directly linked to Tat2 permease**  
412 **but independent on nitrogen source regulation.** In yeast, tryptophan is primarily  
413 transported by one of two permeases, the general amino acid permease, Gap1, and the  
414 high affinity specific Trp-permease, Tat2 (45). In media containing high ammonium  
415 levels, such as SD, Gap1 is not expressed; therefore, we hypothesized that the *chs5Δ*  
416 defect could be associated with defects in Tat2 localization or function. Consistent with  
417 this hypothesis, overexpression of *TAT2* suppressed the ammonium sensitivity of *chs5Δ*  
418 (Figure S1C). These results strongly suggest that ammonium and tryptophan  
419 phenotypes observed in *chs5Δ* are caused by defective function of Tat2 permease.  
420 Notably, the ammonium sensitivity of the double mutant *tat2Δ chs5Δ* was not fully  
421 suppressed by external tryptophan (Figure S1C, D), suggesting that the absence of  
422 exomer may affect additional amino acid transporters. This conclusion is consistent  
423 with the partial alleviation of ammonium sensitivity after *LEU2* introduction (Figure  
424 S1B). As an additional test of the effect of exomer on amino acid transporters, we  
425 analyzed the sensitivity of exomer mutants to toxic analogs of different amino acids  
426 (46-50). Sensitivity to these analogs can indicate changes in the plasma membrane  
427 levels or activity of the relevant amino acid transporter. In the X2180 background, the  
428 exomer mutant *chs5Δ* was moderately more sensitive to the arginine analogue  
429 Canavanine, but significantly more resistant to the proline analogue AzC, to the *HIS3*  
430 inhibitor 3-AT and to toxic concentrations of histidine (Figure 1D). These results are  
431 consistent with a potential defect in the uptake of several amino acids, owing to a defect  
432 in the localization or function of several amino acid permeases (AAPs).

433 Alternatively, the observed phenotypes could simply reflect a defect in the  
434 regulation of nitrogen metabolism in the absence of exomer. To test this possibility, we  
435 first investigated whether the *chs5Δ* mutant showed altered signaling through the

436 Ssy1p-Ptr3p-Ssy5 (SPS) sensor of extracellular amino acids (45) (Figure S2B). We first  
437 compared the phenotypes of the cells lacking SPS to those of cells lacking exomer. We  
438 found that the phenotype of *ssy1Δ*, the core SPS sensor, was not identical to that of  
439 *chs5Δ*. Unlike *chs5Δ*, *ssy1Δ* was resistant to canavanine and sensitive to 3-AT, although  
440 similar to *chs5Δ* it was resistant to AzC (Figure S2A). Moreover, *chs5Δ ssy1Δ* double  
441 mutant exhibited phenotypes of sensitivity to canavanine and resistance to AzC, 3-AT  
442 and to toxic concentrations of histidine as that of *chs5Δ*. We then monitored whether  
443 loss of exomer disrupted SPS function. We found that the localization of Ssy1-GFP in  
444 the *chs5Δ* strain was indistinguishable from the wild type (Figure S2C). More  
445 importantly, loss of exomer did not affect the proteolytic processing of the SPS effector  
446 Stp1 in response to amino acids, a key step in the SPS signaling pathway (45) (Figure  
447 1E). Taken together, these observations indicate that the SPS signaling pathway is fully  
448 functional in the absence of exomer.

449 As an additional test for whether exomer controls amino acids signaling, we  
450 investigated the TORC1 pathway, which regulates many AAPs (45). TORC1 signaling  
451 occurs in preferred nitrogen sources like glutamine and during this signaling, two kinase  
452 regulatory subunits, Gtr1 and Tco89, are recruited to the vacuolar membrane, from  
453 where they triggers the phosphorylation of the small ribosomal subunit, Rsp6, and the  
454 Nitrogen Catabolite Repression (NCR) signaling pathway transcription factor, Gln3 (51,  
455 52) (Figure S2D). We found that Gtr1 and Tco89 localized normally at the vacuolar  
456 membrane in the *chs5Δ* mutant (Figure S2E), the phosphorylation timing of Rps6  
457 occurred normally in this mutant upon growth in different nitrogen sources (Figure 1F)  
458 and the levels of Gln3 phosphorylation were indistinguishable from control under  
459 different nutritional conditions (Figure S2F).

460 All of these results strongly indicate that nitrogen signaling occurs normally in  
461 the absence of exomer. We therefore hypothesized that the observed phenotypes might  
462 be associated directly with a defective transport of one or several AAPs.

463  
464 **Exomer is required for proper intracellular traffic of the Tat2 and Mup1**  
465 **permeases.** In order to test this hypothesis, we first monitored the localization of the  
466 amino acid permeases Tat2 and Mup1. These proteins localized at the PM in induction  
467 media under steady-state conditions (Figure 2A) in either the wild-type or *chs5Δ* mutant  
468 strains. However, in the *chs5Δ* mutant, Tat2 was conspicuously absent at the vacuole  
469 and some of the protein was localized in intracellular spots. Similarly, Mup1 was also

470 localized in intracellular spots in the absence of exomer. Terminally-tagged versions of  
471 Tat2 show impaired endocytosis (see materials and methods section and references  
472 therein). Therefore, to confirm whether Tat2 localization changes in *chs5Δ*, we  
473 performed subcellular fractionations using an internally HA-tagged version of Tat2  
474 (Figure 2B). In the wild-type strain, Tat2-3xHA localized primarily in the lightest  
475 fractions of the gradient together with Pma1, a marker of the plasma membrane fraction.  
476 However, in the *chs5Δ* mutant Tat2-3xHA showed a bimodal distribution, with part of  
477 the protein co-migrating with Pma1 and the other significant part co-migrating with the  
478 TGN/endosomal marker Pep12 in the heavier fractions. These observations suggest that  
479 *chs5Δ* causes partial intracellular accumulation of Tat2 and Mup1 at the  
480 TGN/endosomal compartment. This event would lead to a reduction in the levels of the  
481 permeases at the PM, leading to the tryptophan and amino acid analog responses  
482 described above.

483 The steady state localization of AAPs reflects the balance of anterograde  
484 transport of newly synthesized proteins, endocytosis, and recycling. Therefore, the  
485 mislocalization of Tat2 or Mup1 could reflect a defect in any of these steps. To test  
486 whether exomer contributes to anterograde traffic of Tat2 and Mup1, we used a  
487 regulated expression system based on the GAL1 promoter. Growth on galactose induces  
488 expression thus allowing us to examine anterograde transport based on the arrival of  
489 each permease at the PM. One hour after induction, both proteins were readily apparent  
490 at the plasma membrane in both wild-type and *chs5Δ* cells, suggesting that the overall  
491 rate of anterograde traffic is not dramatically reduced in *chs5Δ* cells (Figure 2C).  
492 However, both Tat2 and Mup1 were less polarized in the *chs5Δ* mutant. In wild-type  
493 cells, both Tat2 and Mup1 were highly polarized in the growing bud, whereas in the  
494 *chs5Δ* mutant a significant amount of each transporter was observed spread along the  
495 PM of the mother cell. A quantitative analysis of Tat2 and Mup1 distribution indicated  
496 that the PM signal in the daughter cells is significantly reduced in the absence of the  
497 exomer for both proteins (Figure 2D). Although the functional significance of the defect  
498 in polarized distribution is unclear, these results indicate that exomer contributes to the  
499 polarized delivery of these proteins to the PM, in a similar fashion to what has been  
500 described for Ena1 (42).

501 Following on, we examined the effect of exomer on the behavior of AAPs after  
502 endocytosis. Tat2 is endocytosed after the depletion of tryptophan from the media and  
503 trafficked to the vacuole for degradation (53). In a wild-type strain, Tat2-GFP signal

504 was increased in the vacuole after tryptophan depletion and the total amount of the  
505 protein was significantly reduced (Figure 2E). However, in the *chs5Δ* mutant,  
506 fluorescence in the vacuole was reduced compared to the wild type, and intracellular  
507 spots became more numerous and intense (Figure 2E). In addition, the total amount of  
508 Tat2 was significantly higher in the *chs5Δ* mutant than in the wild type after tryptophan  
509 depletion. Mup1 is also rapidly endocytosed, trafficked to the vacuole and degraded in  
510 presence of an excess of methionine in wild-type cells (Figure 2F) (54). Similar to Tat2,  
511 in cells lacking exomer Mup1 traffic to the vacuole was reduced 20 minutes after  
512 adding methionine, with fewer cells showing vacuolar fluorescence and more cells  
513 showing substantial plasma membrane signal in the *chs5Δ* mutant compared to the wild  
514 type. This defect was associated with an increase in the number of cells with bright  
515 intracellular spots. However, vacuolar localization was apparent in *chs5Δ* after 45  
516 minutes. Analysis of the total levels of Mup1 by Western blot after adding methionine  
517 indicated that protein degradation was significantly delayed in the absence of exomer  
518 (Figure 2F). These results are consistent with a function for exomer in the proper traffic  
519 of AAPs, and may explain the phenotypes associated with *chs5Δ* in terms of the cells  
520 being sensitive to different levels of tryptophan and toxic amino acids.

521  
522 **Exomer dependent recycling of Tat2 differs from that of Chs3.** Based on the  
523 proposed role of exomer in the recycling of Chs3 (27), we tested whether exomer  
524 controlled the recycling of Tat2. In yeast, the recycling of Tat2 and Mup1 depends on  
525 the f-box protein Rcy1 (55). To determine whether exomer contributes to this step in  
526 recycling, we first compared the phenotypes of *rcy1Δ* and *chs5Δ* mutants. We found  
527 that *rcy1Δ* was sensitive to ammonium, and, as previously reported, required an external  
528 supply of tryptophan for growth (55) (Figure 3A,B). These results are consistent with a  
529 model that proposes that both exomer and Rcy1 may participate in the recycling of  
530 AAPs. Interestingly, the double *rcy1Δ chs5Δ* mutant required a greater concentration of  
531 tryptophan for growth than the single-gene deletion mutants, which could suggest Rcy1  
532 and exomer act at different steps in recycling or that the recycling pathway is only  
533 partially functional in the absence of either factor (Figure 3B).

534 To distinguish between these possibilities, we explored the genetic interactions  
535 between *chs5Δ* and *rcy1Δ* and additional regulators of Tat2. We first examined clathrin  
536 adaptors Gga1 and Gga2, which alter cell surface levels of Tat2 in some mutant  
537 backgrounds by controlling sorting from the TGN to the vacuole (36). We found that



538 *chs5Δ* and *rcy1Δ* showed different effects when combined with deletion of *gga2Δ*, or  
539 the *gga1Δ gga2Δ* double mutant (Figure 3C). The ammonium sensitivity of *chs5Δ* was  
540 suppressed by *gga2Δ* and more so by the *gga1Δ gga2Δ* double mutation. In contrast, the  
541 *rcy1Δ* phenotype was not suppressed by *gga2Δ*. Interestingly, the *gga1Δ* mutant was  
542 sensitive to ammonium on its own, a sensitivity that was additive with the *chs5Δ*  
543 mutant, but not with the *rcy1Δ* mutant. Together these results suggest that exomer and  
544 Rcy1 may affect different steps of AAPs trafficking.

545 The suppression of the ammonium sensitivity of *chs5Δ* by *gga2Δ* is reminiscent  
546 of the previously reported suppression of the calcofluor resistance of *chs5Δ* by *gga2Δ*  
547 (27, 56). We therefore sought to determine whether the exomer-mediated traffic of Tat2  
548 was similar to the exomer-mediated traffic of Chs3. In addition to Gga1 and Gga2, the  
549 clathrin adaptor protein complex AP-1 alters the traffic of Chs3 in exomer mutant cells  
550 (27). We first asked whether deletion of the small subunit of AP-1 (*aps1Δ*) suppressed  
551 the ammonium sensitivity of *chs5Δ*. Unlike calcofluor resistance, *aps1Δ* did not  
552 suppress the ammonium sensitivity of *chs5Δ* (Figure 3D). Similarly, *aps1Δ* did not  
553 suppress the sensitivity of *chs5Δ* to low tryptophan while *gga2Δ* did it efficiently  
554 (Figure S3), suggesting that the traffic of Chs3 and AAPs are strikingly different.

555 To further explore the differential requirements for Chs3 and AAP traffic, we  
556 explored the role of the arrestin family of ubiquitin ligase adaptors because the  
557 recycling of Tat2 is controlled by its ubiquitination mediated by the Bull1 arrestin-like  
558 protein (57). Accordingly, *bull1Δ* suppressed the ammonium sensitivity of the *chs5Δ*  
559 mutant (Figure 3A). In contrast, after analyzing calcofluor sensitivity and staining, the  
560 deletion of *BULL1* did not restore Chs3 PM transport in the *chs5Δ* mutant (Figure 3A, E).  
561 Because Bull1 is one of a number of arrestin-like adaptors, we also tested the partially  
562 redundant Bul2 ligase, the *bull1Δ bul2Δ* double mutant, and individual deletions of ten  
563 additional arrestin ligases. None of the arrestin mutants suppressed the calcofluor  
564 resistance of *chs5Δ*, highlighting the difference between AAPs and Chs3 (See Figure  
565 S4). In summary, while both Tat2 and Chs3 proteins can be re-routed by Gga2 proteins  
566 in the absence of exomer, the two proteins likely diverge at one or more steps in their  
567 traffic, suggesting that the mechanistic requirement for exomer differs for the two  
568 proteins.

569

570 **Exomer is involved in traffic to late endosomes by modulating the proper**  
571 **assembly of the clathrin adaptor complexes.** Exomer and clathrin adaptors mediate

572 the traffic of common cargoes including Chs3 and AAPs, however, their functions  
573 appear to be largely antagonistic to one another. Mechanistically, this antagonism could  
574 be explained by direct physical competition between exomer and clathrin adaptors for  
575 cargo, or something more complex. In order to understand the antagonistic roles of  
576 exomer and clathrin adaptors, we explored their proximity to one another using bi-  
577 molecular fluorescence complementation (BIFC) (39). Exomer comes into close  
578 proximity to both AP-1 and Gga2, based on the appearance of fluorescent puncta in  
579 strains containing Chs5-VN and either Apl4-VC or Gga2-VC. Our BIFC results also  
580 confirmed the previously reported physical interaction of exomer with its cargo Chs3  
581 (Figure 4A), but also revealed close proximity of exomer with Mup1 (Figure 4A),  
582 suggesting exomer may play a direct role in Mup1 traffic.

583 Because BIFC can trap transient proximity between proteins and does not report  
584 on the dynamic changes in protein localization, we next addressed the dynamic TGN  
585 localization of exomer and clathrin adaptors using two-channel spinning disk-confocal  
586 microscopy (Figure 4B, Figure S5). Previous work has established an ordered  
587 recruitment of clathrin adaptors, with Gga2 reaching peak fluorescence several seconds  
588 before AP-1 (6, 58). We found that exomer is recruited shortly after GGA, and  
589 significantly before (21.9 seconds) AP-1 (Figure 4B), a temporal distribution that  
590 overlaps with both clathrin adaptor complexes. This distribution is also consistent with  
591 the co-localization observed between exomer and GGA and AP-1 complexes (Figure  
592 S5E).

593 Next, we explored whether the absence of exomer affected the localization of  
594 clathrin adaptors. In the *chs5Δ* mutant, Gga2 collapsed in significantly brighter and  
595 larger puncta compared to wild-type cells (Figure 4C,D) and similar results were  
596 observed for the AP-1 (Apl4) complex. Moreover, co-localization between Gga2 and  
597 Apl4 was significantly increased in the *chs5Δ* mutant compared with the control (Figure  
598 4C,E).

599 In order to confirm the physiological relevance of these defects, we determined  
600 the sensitivity of the *chs5Δ* mutant to sertraline and myriocin. These drugs affect  
601 membrane fluidity and lipid biosynthesis, and selectively inhibit the growth of yeast  
602 with impaired AP-1 functions (59, 60). We found that *chs5Δ* mutant was significantly  
603 more sensitive to both drugs, showing a half maximal inhibitory concentration (IC50) of  
604  $0.087 \pm 0.005$  mM and  $6.60 \pm 0.33$  mM to myriocin and sertraline respectively, IC50s  
605 significantly ( $p < 0.01$ ) lower than those observed for the wild-type strain ( $0.178 \pm 0.011$

606 mM and  $8.16 \pm 0.19$  mM). This increased sensitivity to both drugs is consistent with  
607 altered AP-1 function in the *chs5Δ* mutant (Figure 4F).

608

609 **Re-exploring the functional link between Arf1 GTPase and the exomer**  
610 **complex.** Exomer was described as an Arf1 GTPase-dependent protein complex (13,15)  
611 and was later co-crystallized with Arf1 (14). Interestingly, TGN clathrin adaptors also  
612 bind Arf1 GTPase (6, 20). Therefore, the antagonistic functions of these complexes may  
613 be through direct competition for active Arf1.

614 We next sought to monitor the effects of exomer on Arf1 localization.  
615 Unfortunately, GFP tagging of Arf1 disrupts its function (61) and alters TGN/EE  
616 morphology (Figure S6A), similarly to what has been described for the null mutant  
617 (62). We therefore analyzed as an alternative the localization of Sec7, a guanine  
618 nucleotide exchange factor (GEF) that stimulates Arf1 activity at the TGN (63)  
619 promoting clathrin adaptor localization (6). We found that similar to clathrin adaptors,  
620 the intensity and area of Sec7 puncta were greater in the *chs5Δ* mutant (Figure 5A).  
621 Moreover, time-lapse analysis showed that in the exomer mutant *chs5Δ* the Sec7 dots  
622 moved significantly slower and showed reduced track displacement, although the  
623 lifespan of the structures was only slightly increased (Figure 5B, Figure S6B,C). The  
624 functional significance of this altered movement is unclear but, altogether, our results  
625 suggest that exomer could influence the behavior of clathrin adaptors through  
626 Arf1/Sec7. In view of this implication of exomer in Arf1/Sec7 dynamics, we sought to  
627 revisit the role of Arf1/Sec7 in exomer functionality.

628 We first addressed the effect of the *arf1Δ* mutation. Surprisingly this mutant  
629 showed increased levels of chitin based on calcofluor staining (Figure 5C, upper  
630 panels), which were in clear agreement with increased levels of Chs3 at the bud neck  
631 (Figure 5C, lower panels, see arrows and amplified insets), despite the partial  
632 accumulation of part of this protein in aberrant TGN/EE structures (Figure 5C, lower  
633 panels, see arrowheads). The absence of Arf1 reversed the effect of the *chs5Δ* mutation  
634 on calcofluor staining and Chs3 localization as previously described (27), likely  
635 through rerouting Chs3 to the PM in a less polarized fashion (Figure 5C). Similar  
636 results were obtained when we depleted Arf1 by growing the *pGALI-ARF1* strain in  
637 glucose. (Figure 5D, E). Moreover, Arf1 depletion in glucose also relieved the  
638 calcofluor and tryptophan phenotypes associated with the *chs5Δ* mutant (Figure 5D, E  
639 and S6D). Although the effects of Sec7 were difficult to assess due its absence being

640 lethal, the transient depletion of Sec7 in the pGAL-*SEC7* strains after growth in glucose  
641 slightly increased chitin synthesis in the wild-type strain and restored chitin synthesis in  
642 the *chs5Δ* mutant (Figure 5D,E).

643 Interestingly, overexpression of either Arf1 or Sec7 in the wild-type strain after  
644 growth in galactose caused hypersensitivity to calcofluor (Figure 5D), which in the case  
645 of Sec7 could be linked to an increased deposition of chitin towards the bud (Figure  
646 5E). However, the overexpression of either protein did not restore chitin synthesis in  
647 *chs5Δ*. In contrast, overexpression of Sec7, but not of Arf1, alleviated the tryptophan  
648 and ammonium phenotypes of *chs5Δ* mutant (Figure 5D and S6D), suggesting that Sec7  
649 has a different effect on the traffic of amino acid permeases.

650 Finally, given the ability of exomer to influence the localization of clathrin  
651 adaptors, we tested the effect of GGA overexpression on exomer function using the  
652 GAL1 promoter. We found that the overexpression of Gga2 in a wild-type strain  
653 significantly reduced the recruitment of exomer and AP-1 complexes at the TGN  
654 (Figure S7A-D). However, this overexpression did not produce a significant  
655 physiological effect on chitin synthesis or ammonium sensitivity, probably because  
656 Gga2 exerts a pleiotropic effect on both complexes (Figure S7E, F). Remarkably, in the  
657 absence of the exomer complex, overexpression of Gga2 partially recovered chitin  
658 synthesis and diminished sensitivity to ammonium (Figure S7E, F). While the chitin  
659 phenotype could be explained by alteration of the AP-1 complex, which in turn  
660 promotes the aperture of the alternative route for the chitin synthase to the PM, the  
661 ammonium phenotype is probably more complex and likely associated with general  
662 alterations of the TGN.

663 Altogether our results support the existence of a complex network of functional  
664 interactions between Arf1, exomer and clathrin adaptors. Moreover, although it is  
665 known that Arf1 activity favors the polarized delivery of Chs3 by exomer, this activity,  
666 contrary to previous reports (17), was found not to be essential for exomer function  
667 since polarization of Chs3 occurred normally in the absence of Arf1/Sec7 (Figure 5C),  
668 when exomer was still present at the TGN/EE membranes (Figure S6E). In contrast, the  
669 ablation of Arf1/Sec7 function reroutes Chs3 and amino acid permeases to the PM,  
670 independently of exomer, through alternative route/s likely to be associated with the  
671 effects of this ablation in the recruitment of clathrin adaptors (6). Interestingly,  
672 overexpression of Sec7 only had a significant effect on the traffic of amino acid

673 permeases in the absence of exomer, reinforcing our previous findings (see above) that  
674 suggest that different links exists between exomer and Chs3 and amino acid permeases.

675

676 **The intracellular traffic of the exomer bona fide cargoes is dependent on**  
677 **their competitive interactions between exomer and AP-1 complexes.** Previous  
678 studies suggest that exomer assembled by different ChAPs subunits may have  
679 dramatically different functions. The Chs6/Bch2 pair is proposed to directly mediate  
680 association with selected cargoes like Chs3, whereas the Bch1/Bud7 pair contributes to  
681 exomer association with membranes and membrane remodeling together with Arf1 (22-  
682 24). Given the effects of exomer on clathrin adaptors, we revisited the roles of the  
683 different exomer subunits in the traffic of Chs3.

684 In the absence of a functional exomer (*chs5Δ*), or when both members of a  
685 group of ChAP paralogs are deleted (*chs6Δ bch2Δ* or *bch1Δ bud7Δ*), yeast cells become  
686 resistant to calcofluor owing to the intracellular retention of Chs3 (review in (64)).  
687 However, we found that in the complete absence of functional exomer the subcellular  
688 localization of Chs3 differed compared to the loss of the cargo binding paralogs  
689 Chs6/Bch2. In the absence of a functional exomer (*chs5Δ*), Chs3 was found in  
690 significantly brighter puncta compared to the wild type (Figure 6A), similar to what was  
691 observed for Gga2/Apl4 in this mutant (Figure 4C). A similar phenotype was also seen  
692 in the *bch1Δ bud7Δ* double mutant (Figure S8B). However, in the *chs6Δ bch2Δ* mutant,  
693 Chs3 puncta were similar to that of the wild type. This suggests exomer complexes  
694 associated with different ChAPs paralogs may have different effects on Chs3 traffic. We  
695 hypothesized that exomer containing the Chs6 and/or Bch2 paralogs may strictly act as  
696 a cargo receptor whereas the exomer containing Bch1 and/or Bud7 paralogs may have  
697 more general effects on traffic, as described above for AAPs.

698 To test this hypothesis, we explored the effect of the exomer mutants on the  
699 localization of Chs3<sup>L24A</sup> mutant protein which cannot bind the AP-1 complex (25). We  
700 found that *chs5Δ* cells expressing Chs3<sup>L24A</sup> were sensitive to calcofluor white, whereas  
701 *chs6Δ* cells expressing Chs3<sup>L24A</sup> were moderately resistant to the same calcofluor  
702 concentration (Figure 6B). This suggests that in cells lacking Chs5, Chs3<sup>L24A</sup> reaches  
703 the cell surface, while in cells lacking Chs6 Chs3<sup>L24A</sup> does not reach the plasma  
704 membrane. As an independent confirmation, we monitored the localization of Chs3<sup>L24A</sup>-  
705 GFP in *chs5Δ*, *chs6Δ bch2Δ* and *bch1Δ bud7Δ* cells. We found Chs3<sup>L24A</sup>-GFP on the

706 cell surface in *chs5Δ* and *bch1Δ bud7Δ* cells but not in *chs6Δ bch2Δ* cells, indicating  
707 that the two ChAP paralogous pairs play different roles in Chs3 traffic (Figure S8B).

708 We sought to explore this hypothesis further by examining the localization of  
709 Chs5-Chs3 BIFC complexes in different ChAPs mutant backgrounds. We hypothesized  
710 that if complexes containing Chs6/Bch2 were exclusively required for cargo loading in  
711 exocytic vesicles then the formation of the Chs5-Chs3 BIFC complexes could be able to  
712 bypass this requirement. Surprisingly, we found that Chs5-Chs3 BIFC complexes  
713 localized along the cell surface in both *chs6Δ bch2Δ* or *bch1Δ bud7Δ* cells (Figure 6C,  
714 S8A). However, these BIFC complexes could not reach the PM in the absence of Chs7  
715 (*chs7Δ* strain), a specific chaperon implicated in a Chs3-exocytic step prior to exomer  
716 complex function (37). This suggests that, under this condition, complexes containing  
717 only Bch1/Bud7 are competent for exocytosis, and that exocytosis may not be the only  
718 role of exomer containing Chs6 and Bch2. Consistent with these findings, we found that  
719 the concomitant expression of Chs5-VC and Chs3-VN was able to restore calcofluor  
720 white sensitivity to *chs6Δ* (Figure 6D). Interestingly, the Chs5-Chs3 BIFC complexes  
721 were conspicuously absent from the neck region in both double mutants, *chs6Δ bch2Δ*  
722 and *bch1Δ bud7Δ*, consistent with a lower polarization of the protein similar to the  
723 localization observed for the Chs3<sup>L24A</sup> protein, which is unable to bind the AP-1  
724 complex (Figure S8A).

725 One explanation for these phenotypes is that the artificially stable Chs3-Chs5  
726 dimer induced by BIFC tags prevents AP-1 from retaining Chs3 in the TGN and  
727 therefore the protein can reach the PM without Chs6 or Bch1/Bud7 following an  
728 alternative route (27). To test if the converse could be true, we tested the effect of the  
729 formation of Apl4-Chs3 BIFC complexes on global Chs3 localization. We found Apl4-  
730 Chs3 BIFC complexes were only detected as intracellular dots, consistent with the  
731 intracellular localization of the AP-1 complex (Figure 6E, upper panel). The formation  
732 of these complexes was highly specific because they were clearly altered in the absence  
733 of Gga2 (Figure 6E), a finding that clearly agrees with the proposed role for GGAs in  
734 the recruitment of AP-1 to the TGN (6). More important, cells expressing these BIFC  
735 complexes were moderately resistant to calcofluor, indicating that artificial stable  
736 interaction of Chs3 with AP-1 reduced the exit of Chs3 to the plasma membrane (Figure  
737 6E, lower panel).

738 Altogether our results suggest that the exomer and AP-1 complexes can compete  
739 for some cargoes in *S. cerevisiae*, such as Chs3, but not others such as AAPs. These

740 findings may be highly relevant and influence our understanding of how protein sorting  
741 at the TGN (see discussion) may have evolved.

742

743 **Exploring the physiological relationship between the exomer and AP-1**  
744 **complexes in *Candida albicans*.** These multiple lines of evidence support the idea of a  
745 TGN niche in where exomer and AP-1 complexes maintain competitive and regulated  
746 relationships between themselves and with respect to their cargoes. Thus, we sought to  
747 analyze whether these relationships have been conserved along evolution. Considering  
748 the evolutionary distribution of the exomer complex (65), we decided to analyze this  
749 relationship in *Candida albicans* where both complexes exist. Given the effect of  
750 exomer on polarized exocytosis in *Saccharomyces cerevisiae*, we examined filamentous  
751 growth which strongly depends on polarized exocytosis. We examined the filamentous  
752 growth of cells lacking exomer and AP-1 in liquid (Figure 7A,B) and on different solid  
753 media (Figure 7C). Surprisingly, loss of exomer only weakly affected filamentous  
754 growth whereas the AP-1 complex was indispensable for hyphal formation on solid  
755 media and its absence strongly reduced the rate of hyphal growth in liquid media.  
756 However, exomer deletion only partially altered the morphology of filaments growing  
757 on solid and in liquid media, and slightly reduces hyphal growth in liquid media.  
758 Interestingly, the double mutant showed additive phenotypes, with stronger alterations  
759 in colony morphology and a lower hyphal extension rate in liquid media. These results  
760 highlight the significant differences between the role of the exomer and AP-1  
761 complexes in yeast or hyphal cells, and suggest that the AP-1 complex has an important  
762 role in maintaining polarity during mycelial growth.

763

764

## 765 **DISCUSSION**

766

767 **Exomer facilitates the polarized delivery of several proteins to the PM.** The  
768 TGN is a major platform for the intracellular sorting of proteins where anterograde and  
769 recycling pathways converge (3, 66). Surprisingly, even in yeast, the mechanisms for  
770 protein sorting to the PM remain unclear (2). Some years ago, the discovery of exomer  
771 as an adaptor complex at the TGN, required for the delivery of Chs3 to the PM (17, 21),  
772 opened a pathway to study these mechanisms. However, the number of proteins that  
773 depend on exomer for their transport is limited, this observation was striking given the

774 evolutionary maintenance of this sophisticated machinery. Moreover, the phenotypes of  
775 mutants lacking exomer, as well as the range of its genetic interaction, suggested  
776 additional roles in protein trafficking (21, 42).

777 The characterization of the sensitivity of exomer mutants to ammonium ((21  
778 and this work) expands the previously reported role of exomer in protein traffic  
779 regulation. Here, we have shown that the ammonium sensitivity of exomer mutants is  
780 linked to the absence of the unique scaffold Chs5 or the pair of ChAPs Bch1/Bud7, but  
781 not to the absence of the other pair of ChAPs Chs6/Bch2, which has been described as  
782 cargo adaptor for the Chs3 and Pin2 proteins (22, 23). This suggests additional  
783 functions for exomer containing Bch1/Bud7 that are independent of the cargo binding  
784 ChAPs.

785 Our work unequivocally links the ammonium hypersensitivity of the exomer  
786 mutant *chs5* $\Delta$  to a deficient uptake of tryptophan. Still, our results also suggest that the  
787 absence of exomer affects the uptake of other amino acids, based on the partial  
788 alleviation of *chs5* $\Delta$  ammonium sensitivity by the *LEU2* gene, or the altered sensitivity  
789 to several amino acid analogs. These defects on amino acid uptake are not caused by  
790 deficient signaling through the major signaling pathways involved in nitrogen  
791 assimilation. Rather, the ammonium sensitivity is directly linked to defective traffic of  
792 the tryptophan permease Tat2 in the *chs5* $\Delta$  mutant. This traffic defect is shared with the  
793 Mup1 permease and the sodium ATPase Ena1 (42). Therefore, our results highlight the  
794 involvement of exomer in the polarized traffic of these three proteins, and likely other  
795 transporters. This specific function in polarized transport explains why these proteins  
796 have not been previously linked to exomer function, since their transport to the plasma  
797 membrane is not blocked in the absence of exomer and the defects in polarization, much  
798 more discrete, were only detectable after the use of regulatable promoters. Therefore,  
799 our work enlarges the spectrum of proteins that rely on exomer for polarized transport.  
800 Moreover, the results presented here link this transport to the Bch1/Bud7 pair of  
801 ChAPs. These subunits lack the cargo binding activity of the Chs6/Bch2 (22, 23),  
802 suggesting that exomer may also contribute to the transport of proteins through its  
803 action in coat assembly in addition to its direct role as cargo adaptor. Since Bch1/Bud7  
804 are less divergent from the ChAP representative found in the root of the fungal  
805 evolutionary tree, this may suggest this coat function is the ancestral role of the complex  
806 (29, 65).

807



808 **Exomer contributes to late endosomal traffic of several proteins through its**  
809 **functional relationship with clathrin adaptor complexes.** Our results show that  
810 *chs5Δ* disrupts not only the anterograde transport of Tat2 and Mup1 to the PM but also  
811 their traffic to the vacuole. This defect is consistent with the overall alterations of the  
812 TGN dynamics associated with the modified recruitment of clathrin adaptor complexes  
813 at TGN membranes in the absence of exomer. Notably, a similar cooperation between  
814 exomer and clathrin adaptors was previously reported in *S. pombe* (30). The deletion of  
815 the GGA complex suppressed both the ammonium sensitivity and the tryptophan  
816 requirement of the *chs5Δ* mutant. This most likely occurred by reducing Tat2 traffic to  
817 the vacuole, thereby restoring its delivery to the plasma membrane (36). Surprisingly,  
818 the absence of the AP-1 complex had only a marginal effect on *chs5Δ* phenotypes  
819 linked to tryptophan transport, suggesting that AP-1 is not linked to Tat2 traffic.  
820 Interestingly, exomer does not seem to affect the early endosomal recycling of Ta2 that  
821 is mediated by Rcy1 (55) because the effects of the absence of Rcy1 and Chs5 are  
822 additive. In addition, the deletions of *GGA1* or *GGA2* have opposite effects on the  
823 ammonium sensitivity of the *rcy1Δ* or *chs5Δ* mutants. Altogether, these results indicate  
824 that the absence of exomer affects the late endosomal traffic of Tat2 without affecting  
825 its Rcy1-dependent early endosomal recycling (55).

826 Exomer and clathrin adaptor complexes localize and mediate sorting decisions at  
827 the TGN, but also rely on the function of Arf1 GTPase for proper functioning (21, 67).  
828 Our results support a model where both exomer and clathrin adaptor complexes would  
829 compete for Arf1 based on several lines of evidence. The absence of exomer altered the  
830 dynamics of the clathrin adaptor complexes similar to previously reported effects of  
831 *Pik1/Frq1* overexpression, which is thought to upregulate Arf1 activity (6). In  
832 agreement with this evidence, the overexpression of *Gga2*, which may reduce available  
833 levels of Arf1, reduced the effective recruitment of Chs5 to the TGN membranes  
834 (Figure S7A). In addition, overexpression of Arf1 or *Sec7* increased chitin synthesis,  
835 which is dependent on the presence of a functional exomer, in clear agreement with the  
836 regulatory role on exomer function proposed for Arf1 (17, 21, 27). Moreover, this  
837 model is also compatible with the action of exomer as an inhibitor of Arf-GAP (GTPase  
838 activating protein) activity, as previously proposed (20). Accordingly, overexpression of  
839 Arf1/*Sec7* did not suppress the chitin synthesis defect associated with the *chs5Δ* mutant.  
840 By contrast, depletion of Arf1 or *Sec7* effectively suppressed the *chs5Δ*-associated  
841 phenotypes, most likely by disrupting clathrin-mediated TGN-endosome traffic (27).

842 Interestingly, overexpression of Sec7 alleviated partially the ammonium sensitivity and  
843 the tryptophan requirement of the *chs5Δ* mutant, indicating that Chs3 and Tat2 may  
844 follow different itineraries from the TGN.

845 One unexpected finding of this work is the observation that the polarized  
846 delivery of Chs3 is unaffected by the absence of Arf1. This is surprising because  
847 polarized delivery of Chs3 depends on the presence of a functional exomer, which  
848 should be disrupted when Arf1 is depleted. This result is indicative of the assembly of a  
849 functional exomer complex despite the strong morphological alteration of the TGN in  
850 the *arf1Δ* mutant. This somehow contradicts previous indirect observations suggesting  
851 that Arf1 is required for exomer assembly (17, 21). Whether this observation is  
852 explained by the function of Arf2 or other GTPase still remains to be established.

853 Altogether our results, together with those previously reported (30), show that in  
854 addition to the described role of exomer in the anterograde transport of proteins exomer  
855 also contributes to the late endosomal traffic of multiple proteins by facilitating the  
856 proper functioning of the clathrin adaptor complexes. This function appears to be  
857 independent of the cargo binding activity of exomer, and may vastly increase the  
858 number of proteins known to depend on exomer for localization.

859  
860 **Exomer and AP-1 complexes compete for a subset of cargoes.** An interesting  
861 reported here observation is the differential effect of the AP-1 complex on the traffic of  
862 exomer-dependent proteins. Our phenotypic analysis showed that deletion of AP-1  
863 complex has little effect on Tat2 traffic in the *chs5Δ* mutants, which is similar to prior  
864 reports about Ena1 (42). By contrast, the absence of AP-1 efficiently reroutes Chs3, as  
865 well as the other bona fide cargoes, Fus1 and Pin2, to the PM in the absence of exomer  
866 (18, 19). This can be simply explained by the physical interaction between these cargoes  
867 and both the exomer and AP-1 complexes as it has been shown for Chs3 (25, 26). Our  
868 *in vivo* results favor a mechanistic model in which exomer and AP-1 compete for  
869 cargoes, since the artificially increased interaction between Chs3 and Chs5 through the  
870 BIFC system allows Chs3 traffic to PM avoiding the TGN-retention of Chs3 mediated  
871 by AP-1 in *chs6Δ* and *bch1Δ bud7Δ* mutants. Moreover, tighter binding of Chs3 to AP-  
872 1 using the BIFC system also reduced Chs3 traffic to the PM (Figure 6).

873 In addition to the direct competition between exomer and AP-1 for cargoes, we  
874 propose that competition for Arf1 also contributes to their complex interaction. Exomer  
875 and CCV are assembled at the TGN in close proximity ((58), and this work), and both

876 utilize Arf1 (Figure 7D). Moreover, exomer is strictly required for the PM delivery of a  
877 restricted number of cargoes that are recycled to the TGN through their physical  
878 interaction with the AP-1 complex (Figure 7E). However, exomer also facilitates the  
879 polarized delivery of other proteins that recycle independently of AP-1. Additionally,  
880 exomer contributes to the proper assembly of the clathrin adaptor complexes that  
881 facilitate late endosomal traffic of multiple proteins. Functional disruption of clathrin  
882 adaptor complexes reroutes proteins into alternative non-polarized ways to the PM.  
883 Our results also discriminate between the functions of the GGA and AP-1 complexes at  
884 the TGN in *S. cerevisiae*, a subject still under debate. The role of AP-1 in *S. cerevisiae*  
885 appears limited, affecting only a restricted number of cargoes that are recycled by this  
886 complex through their direct binding. The GGA complex appears to perform more  
887 general functions in the organization of the TGN. This occurs independently of the  
888 specific recognition of the cargoes (6) thus affecting the late endosomal traffic of  
889 several proteins (68-70). This view is similar to what has been proposed for animal  
890 cells, in which AP-1 would have a distinct role in the protein recycling that is not shared  
891 with GGAs (71).

892 The many functional connections between exomer and AP-1 found in yeasts  
893 help to raise the interesting question of whether these are evolutionarily conserved  
894 relationships. Our work with *C. albicans* (Figure 7A-C and (29)) indicates that while  
895 exomer contributes to the polarization of Chs3 and only displays a secondary role in  
896 filamentous growth, AP-1 is pivotal for this hyperpolarized process (Figure 7F). More  
897 broadly, the absence of AP-1 is lethal in filamentous fungi (72). However, all exomer  
898 mutants characterized are fully viable (29, 30) (M. Riquelme, personal communication),  
899 suggesting that the functional interconnection between exomer and AP-1 may be limited  
900 to yeast cells within the fungal lineage. The AP-1 complex is conserved in eukaryotes  
901 (73), but exomer appears to be fungal specific (65), evidence that is consistent with the  
902 major role of AP-1 in polarized traffic in animal cells (74). Therefore, our results reflect  
903 the general idea that polarity determinants (2), and thus the mechanism of sorting at the  
904 TGN, are highly diverse, coexisting mechanisms based on cargo adaptor complexes  
905 together with others based on protein partitioning between micro-domains, with exomer  
906 somehow exerting both functions in yeast depending on the cargo to be sorted.

907

## 908 **ACKNOWLEDGMENTS**

909

910 We thank A. Spang, J. Ariño and S. Moreno for strains and reagents and for the  
911 many useful discussions that took place throughout this work and to E. Keck for the  
912 editorial correction of the manuscript. We especially acknowledge the initial work  
913 carried out by M. Berroa on *C. albicans*. CAP was supported by a University of  
914 Salamanca (USAL) predoctoral fellowship, an EMBO short-term fellowship and an  
915 USAL Grant for Excellence; NS was supported by a FPU fellowship from the Spanish  
916 Ministry of Education. Work at the CR laboratory was supported by grants BFU2017-  
917 84508-P from the CICYT/FEDER program (Ministerio de Economía, Industria y  
918 Competitividad, Gobierno de España) and SA116G19 from Consejería de Educación,  
919 Junta de Castilla y León. JMM laboratory was supported by grants RTC-2017-6468-2-  
920 AR and BIO2016-77776-P (Ministerio de Economía, Industria y Competitividad,  
921 Gobierno de España) and work by MCD was supported by the National Institutes of  
922 Health (USA) grant R01 GM092741 and by funds from the Michigan Protein Folding  
923 Disease Initiative. CR also thanks the financial support awarded to the Institute of  
924 Biological and Functional Genomics (IBFG) (CLU-2017-03) provided by the Junta de  
925 Castilla y León through the program "Escalera de Excelencia", co-financed by the P.O.  
926 FEDER of Castilla y León 14-20.

927

## 928 **CONFLICT OF INTEREST STATMENT**

929

930 The authors state explicitly there are no conflicts of interest in connection with  
931 this article.

932

## 933 **AUTHOR CONTRIBUTIONS**

934

935 CR and CAP designed the research and CAP performed most of the  
936 experiments. NS, RV, JMM and MCD did experimental work and/or provided essential  
937 reagents. CR and CAP wrote the paper and generated the figures. MCD contributed to  
938 the final text editing. All authors have read and approved the final manuscript.

939

## 940 **REFERENCES**

941

- 942 1. De Matteis, M. A., and Luini, A. (2008) Exiting the Golgi complex. *Nat Rev*  
943 *Mol Cell Biol* **9**, 273-284
- 944 2. Bonifacino, J. S. (2014) Adaptor proteins involved in polarized sorting. *J Cell*  
945 *Biol* **204**, 7-17
- 946 3. Guo, Y., Sirkis, D. W., and Schekman, R. (2014) Protein sorting at the trans-  
947 Golgi network. *Annu Rev Cell Dev Biol* **30**, 169-206
- 948 4. Robinson, M. S. (2015) Forty Years of Clathrin-coated Vesicles. *Traffic* **16**,  
949 1210-1238
- 950 5. Traub, L. M. (2005) Common principles in clathrin-mediated sorting at the  
951 Golgi and the plasma membrane. *Biochem Biophys Acta* **1744**, 415-437
- 952 6. Daboussi, L., Costaguta, G., and Payne, G. S. (2012) Phosphoinositide-mediated  
953 clathrin adaptor progression at the trans-Golgi network. *Nat Cell Biol* **14**, 239-  
954 248
- 955 7. Becuwe, M., and Leon, S. (2014) Integrated control of transporter endocytosis  
956 and recycling by the arrestin-related protein Rod1 and the ubiquitin ligase Rsp5.  
957 *eLife* **3**
- 958 8. Scott, P. M., Bilodeau, P. S., Zhdankina, O., Winistorfer, S. C., Hauglund, M. J.,  
959 Allaman, M. M., Kearney, W. R., Robertson, A. D., Boman, A. L., and Piper, R.  
960 C. (2004) GGA proteins bind ubiquitin to facilitate sorting at the trans-Golgi  
961 network. *Nature cell biology* **6**, 252-259
- 962 9. Deng, Y., Guo, Y., Watson, H., Au, W. C., Shakoury-Elizeh, M., Basrai, M. A.,  
963 Bonifacino, J. S., and Philpott, C. C. (2009) Gga2 mediates sequential ubiquitin-  
964 independent and ubiquitin-dependent steps in the trafficking of ARN1 from the  
965 trans-Golgi network to the vacuole. *The Journal of biological chemistry* **284**,  
966 23830-23841
- 967 10. Stringer, D. K., and Piper, R. C. (2011) A single ubiquitin is sufficient for cargo  
968 protein entry into MVBs in the absence of ESCRT ubiquitination. *J Cell Biol*  
969 **192**, 229-242
- 970 11. Ha, S. A., Torabinejad, J., DeWald, D., B., Wenk, M. R., Lucas, t. L., De  
971 Camilli, P., Newitt, R. A., Aebersold, R., and Nothwehr, S. F. (2003) The  
972 synaptojanin-like protein Inp53/Sjl3 functions with clathrin in a yeast TGN-to-  
973 endosome pathway distinct from the GGA protein-dependent pathway. *Mol Biol*  
974 *Cell* **14**, 1319-1333

- 975 12. Marcusson, E. G., Horazdovsky, B. F., Cereghino, J. L., Gharakhanian, E., and  
976 Emr, S. D. (1994) The sorting receptor for yeast vacuolar carboxypeptidase Y is  
977 encoded by the VPS10 gene. *Cell* **77**, 579-586
- 978 13. Yeung, B. G., and Payne, G. S. (2001) Clathrin interactions with C-terminal  
979 regions of the yeast AP-1 beta and gamma subunits are important for AP-1  
980 association with clathrin coats. *Traffic* **2**, 565-576
- 981 14. Gall, W. E., Geething, N. C., Hua, Z., Ingram, M. F., Liu, K., Chen, S. I., and  
982 Graham, T. R. (2002) Drs2p-dependent formation of exocytic clathrin-coated  
983 vesicles in vivo. *Curr Biol* **17**, 1623-1627
- 984 15. Santos, B., and Snyder, M. (1997) Targeting of chitin synthase 3 to polarized  
985 growth sites in yeast requires Chs5p and Myo2p. *J. Cell Biol.* **136**, 95-110
- 986 16. Ziman, M., Chuang, J. S., Tsung, M., Hamamoto, S., and Schekman, R. (1998)  
987 Chs6p-dependent anterograde transport of Chs3p from the chitosome to the  
988 plasma membrane in *Saccharomyces cerevisiae*. *Mol. Biol. Cell* **9**, 1565-1576
- 989 17. Wang, C. W., Hamamoto, S., Orci, L., and Schekman, R. (2006) Exomer: A  
990 coat complex for transport of select membrane proteins from the trans-Golgi  
991 network to the plasma membrane in yeast. *J. Cell Biol.* **174**, 973-983
- 992 18. Barfield, R. M., Fromme, J. C., and Schekman, R. (2009) The exomer coat  
993 complex transports Fus1p to the plasma membrane via a novel plasma  
994 membrane sorting signal in yeast. *Mol. Biol. Cell* **20**, 4985-4996
- 995 19. Ritz, A. M., Trautwein, M., Grassinger, F., and Spang, A. (2014) The prion-like  
996 domain in the exomer-dependent cargo Pin2 serves as a trans-Golgi retention  
997 motif. *Cell Rep* **10**, 249-260
- 998 20. Paczkowski, J. E., Richardson, B. C., Strassner, A. M., and Fromme, J. C.  
999 (2012) The exomer cargo adaptor structure reveals a novel GTPase-binding  
1000 domain. *EMBO J.* **31**, 4191-4203
- 1001 21. Trautwein, M., Schindler, C., Gauss, R., Dengjel, J., Hartmann, E., and Spang,  
1002 A. (2006) Arf1p, Chs5p and the ChAPs are required for export of specialized  
1003 cargo from the Golgi. *EMBO J* **25**, 943-954
- 1004 22. Paczkowski, J. E., and Fromme, J. C. (2014) Structural basis for membrane  
1005 binding and remodeling by the exomer secretory vesicle cargo adaptor. *Dev Cell*  
1006 **30**, 610-624

- 1007 23. Huranova, M., Muruganandam, G., Weiss, M., and Spang, A. (2016) Dynamic  
1008 assembly of the exomer secretory vesicle cargo adaptor subunits. *EMBO Rep* **17**,  
1009 202-219
- 1010 24. Rockenbauch, U., Ritz, A. M., Sacristan, C., Roncero, C., and Spang, A. (2012)  
1011 The complex interactions of Chs5p, the ChAPs, and the cargo Chs3p. *Mol Biol*  
1012 *Cell* **23**, 4404-44015
- 1013 25. Starr, T. L., Pagant, S., Wang, C. W., and Schekman, R. (2012) Sorting Signals  
1014 That Mediate Traffic of Chitin Synthase III between the TGN/Endosomes and to  
1015 the Plasma Membrane in Yeast. *PLoS One* **7**, e46386. doi: 46310.41371/
- 1016 26. Weiskoff, A. M., and Fromme, J. C. (2014) Distinct N-terminal regions of the  
1017 exomer secretory vesicle cargo Chs3 regulate its trafficking itinerary. *Front Cell*  
1018 *Dev Biol* **2:47**, doi: 10.3389/fcell.2014.00047
- 1019 27. Valdivia, R. H., Baggot, D., Chuang, J. S., and Schekman, R. (2002) The yeast  
1020 Clathrin adaptor protein complex 1 is required for the efficient retention of a  
1021 subset of late Golgi membrane proteins. *Dev. Cell* **2**, 283-294
- 1022 28. Zanolari, B., Rockenbauch, U., Trautwein, M., Clay, L., Barral, Y., and Spang,  
1023 A. (2011) Transport to the plasma membrane is regulated differently early and  
1024 late in the cell cycle in *Saccharomyces cerevisiae*. *J. Cell Sci.* **124**, 1055-1066
- 1025 29. Anton, C., Valdez Taubas, J., and Roncero, C. (2018) The Functional  
1026 Specialization of Exomer as a Cargo Adaptor During the Evolution of Fungi.  
1027 *Genetics* **208**, 1483-1498
- 1028 30. Hoya, M., Yanguas, F., Moro, S., Prescianotto-Baschong, C., Doncel, C., de  
1029 León, N., Curto, M. Á., Spang, A., and Valdivieso, M. H. (2017) Traffic  
1030 Through the Trans-Golgi Network and the Endosomal System Requires  
1031 Collaboration Between Exomer and Clathrin Adaptors in Fission Yeast.  
1032 *Genetics* **205**, 673-690
- 1033 31. Rose, M. D., Wisnton, F., and Hieter, P. (1990) *Methods in Yeast Genetics: A*  
1034 *Laboratory Course Manual.*, Cold Spring Harbor Laboratory Press, New York
- 1035 32. Goldstein, A. L., and McCusker, J. H. (1999) Three new dominant drug  
1036 resistance cassettes for gene disruption in *Saccharomyces cerevisiae*. *Yeast* **15**,  
1037 1541-1553
- 1038 33. Longtine, M. S., McKenzie, A. r., Demarini, D. J., Shah, N. G., Wach, A.,  
1039 Brachat, A., Philippsen, P., and Pringle, J. R. (1998) Additional modules for

- 1040 versatile and economical PCR-based gene deletion and modification in  
1041 *Saccharomyces cerevisiae*. *Yeast*. **14**, 953-961
- 1042 34. Sato, M., Dhut, S., and Toda, T. (2005) New drug-resistant cassettes for gene  
1043 disruption and epitope tagging in *Schizosaccharomyces pombe*. *Yeast* **22**, 582-  
1044 591
- 1045 35. Stuckey, S., Mukherjee, K., and Storici, F. (2011) In vivo site-specific  
1046 mutagenesis and gene collage using the delitto perfetto system in yeast  
1047 *Saccharomyces cerevisiae*. *Methods Mol Biol* **745**, 173-191
- 1048 36. Hachiro, T., Yamamoto, T., Nakano, K., and Tanaka, K. (2013) Phospholipid  
1049 flippases Lem3p-Dnf1p and Lem3p-Dnf2p are involved in the sorting of the  
1050 tryptophan permease Tat2p in yeast. *J Biol Chem* **288**, 3594-3608
- 1051 37. Trilla, J. A., Duran, A., and Roncero, C. (1999) Chs7p, a new protein involved  
1052 in the control of protein export from the endoplasmic reticulum that is  
1053 specifically engaged in the regulation of chitin synthesis in *Saccharomyces*  
1054 *cerevisiae*. *J. Cell Biol.* **145**, 1153-1163
- 1055 38. Hung, C. W., Martínez-Márquez, J. Y., FT., J., and Duncan, M. C. (2018) A  
1056 simple and inexpensive quantitative technique for determining chemical  
1057 sensitivity in *Saccharomyces cerevisiae*. *Sci Rep* **8**, 11919
- 1058 39. Sung, M. K., and Huh, W. K. (2007) Bimolecular fluorescence complementation  
1059 analysis system for in vivo detection of protein-protein interaction in  
1060 *Saccharomyces cerevisiae*. *Yeast* **24**, 767-775
- 1061 40. Arcones, I., and Roncero, C. (2016) Monitoring chitin deposition during septum  
1062 assembly in budding yeast. *Methods Mol Biol* **1369**, 59-72
- 1063 41. Vicent, I., Navarro, A., Mulet, J. M., Sharma, S., and Serrano, R. (2015) Uptake  
1064 of inorganic phosphate is a limiting factor for *Saccharomyces cerevisiae* during  
1065 growth at low temperatures. *FEMS Yeast Res* **15**, fov008
- 1066 42. Anton, C., Zanolari, B., Arcones, I., Wang, C., Mulet, J. M., Spang, A., and  
1067 Roncero, C. (2017) Involvement of the exomer complex in the polarized  
1068 transport of Ena1 required for *Saccharomyces cerevisiae* survival against toxic  
1069 cations. *Mol Biol Cell* **28**, 3672-3685
- 1070 43. Hess, D. C., Lu, W., Rabinowitz, J. D., and Botstein, D. (2006) Ammonium  
1071 toxicity and potassium limitation in yeast. *PLoS Biol* **4**, e351
- 1072 44. Schmidt, A., Hall, M. N., and Koller, A. (1994) Two FK506 resistance-  
1073 conferring genes in *Saccharomyces cerevisiae*, TAT1 and TAT2, encode amino



- 1074 acid permeases mediating tyrosine and tryptophan uptake. *Mol Cell Biol* **14**,  
1075 6597-6606
- 1076 45. Ljungdahl, P. O., and Daignan-Fornier, B. (2012) Regulation of amino acid,  
1077 nucleotide, and phosphate metabolism in *Saccharomyces cerevisiae*. *Genetics*  
1078 **190**, 885-929
- 1079 46. Ljungdahl, P. O., Gimeno, C. J., Styles, C. A., and Fink, G. R. (1992) SHR3: a  
1080 novel component of the secretory pathway specifically required for localization  
1081 of amino acid permeases in yeast. *Cell* **71**, 463-478
- 1082 47. Kanazawa, S., Driscoll, M., and Struhl, K. (1992) ATR1, a *Saccharomyces*  
1083 *cerevisiae* gene encoding a transmembrane protein required for aminotriazole  
1084 resistance. *Mol Cell Biol* **8**, 664-673
- 1085 48. Wada, M., Okabe, K., Kataoka, M., Shimizu, S., Yokota, A., and Takagi, H.  
1086 (2008) Distribution of L-azetidine-2-carboxylate N-acetyltransferase in yeast.  
1087 *Biosci Biotechnol Biochem* **72**, 582-586
- 1088 49. Falco, S. C., and Dumas, K. S. (1985) Genetic analysis of mutants of  
1089 *Saccharomyces cerevisiae* resistant to the herbicide sulfometuron methyl.  
1090 *Genetics* **109**, 21-35
- 1091 50. Larimer, F. W., Ramey, D. W., Lijinsky, W., and Epler, J. L. (1978)  
1092 Mutagenicity of methylated N-nitrosopiperidines in *Saccharomyces cerevisiae*.  
1093 *Mutat Res* **57**, 155-161
- 1094 51. González, A., Shimobayashi, M., Eisenberg, T., Merle, D. A., Pendl, T., Hall,  
1095 M. N., and Moustafa, T. (2015) TORC1 promotes phosphorylation of ribosomal  
1096 protein S6 via the AGC kinase Ypk3 in *Saccharomyces cerevisiae*. *PLoS One*  
1097 **10**, e0120250
- 1098 52. Zhang, W., Du, G., Zhou, J., and Chen, J. (2018) Regulation of Sensing,  
1099 Transportation, and Catabolism of Nitrogen Sources in *Saccharomyces*  
1100 *cerevisiae*. *Microbiol Mol Biol Rev* **82**, e00040-00017
- 1101 53. Beck, T., Schmidt, A., and Hall, M. N. (1999) Starvation induces vacuolar  
1102 targeting and degradation of the tryptophan permease in yeast. *J Cell Biol* **146**,  
1103 1227-1238
- 1104 54. Menant, A., Barbey, R., and Thomas, D. (2006) Substrate-mediated remodeling  
1105 of methionine transport by multiple ubiquitin-dependent mechanisms in yeast  
1106 cells. *EMBO J* **25**, 4436-4447

- 1107 55. MacDonald, C., and Piper, R. C. (2017) Genetic dissection of early endosomal  
1108 recycling highlights a TORC1-independent role for Rag GTPases. *J Cell Biol*  
1109 **216**, 3275-3290
- 1110 56. Copic, A., Starr, T. L., and Schekman, R. (2007) Ent3p and Ent5p exhibit cargo-  
1111 specific functions in trafficking proteins between the trans-Golgi network and  
1112 the endosomes in yeast. *Mol. Biol. Cell* **18**, 1803-1815
- 1113 57. Abe, F., and H., I. (2003) Pressure-induced differential regulation of the two  
1114 tryptophan permeases Tat1 and Tat2 by ubiquitin ligase Rsp5 and its binding  
1115 proteins, Bul1 and Bul2. *Mol Cell Biol*, 7566-7584
- 1116 58. Tojima, T., Suda, Y., Ishii, M., Kurokawa, K., and Nakano, A. (2019)  
1117 Spatiotemporal dissection of the trans-Golgi network. *J Cell Sci* **132**, jcs231159
- 1118 59. Whitfield, S. T., Burston, H. E., Bean, B. D., Raghuram, N., Maldonado-Báez,  
1119 L., Davey, M., Wendland, B., and Conibear, E. (2016) The alternate AP-1  
1120 adaptor subunit Apm2 interacts with the Mil1 regulatory protein and confers  
1121 differential cargo sorting. *Mol Biol Cell* **27**, 588-598
- 1122 60. Zysnarski, C. J., Lahiri, S., Javed, F. T., Martínez-Márquez, J. Y., Trowbridge,  
1123 J. W., and Duncan, M. C. (2019) Adaptor protein complex-1 (AP-1) is recruited  
1124 by the HEATR5 protein Laa1 and its co-factor Laa2 in yeast. *J Biol Chem* **294**,  
1125 1410-1419
- 1126 61. Jian, X., Cavenagh, M., Gruschus, J. M., Randazzo, P. A., and Kahn, R. A.  
1127 (2010) Modifications to the C-terminus of Arf1 alter cell functions and protein  
1128 interactions. *Traffic* **11**, 732-742
- 1129 62. Gaynor, E. C., Chen, C. Y., Emr, S. D., and Graham, T. R. (1998) ARF is  
1130 required for maintenance of yeast Golgi and endosome structure and function.  
1131 *Mol Biol Cell* **9**, 653-670
- 1132 63. Richardson, B. C., McDonold, C. M., and Fromme, J. C. (2012) The Sec7 Arf-  
1133 GEF is recruited to the trans-Golgi network by positive feedback. *Dev Cell* **22**,  
1134 799-810
- 1135 64. Roncero, C. (2002) The genetic complexity of chitin synthesis in fungi. *Curr*  
1136 *Genet.* **41**, 367-378
- 1137 65. Ramirez-Macias, I., Barlow, L. D., Anton, C., Spang, A., Roncero, C., and  
1138 Dacks, J. B. (2018) Evolutionary cell biology traces de rise of exomer complex  
1139 in Fungi from an ancient eukaryotic component. *Sci Rep* **8**, 11154

- 1140 66. Day, K. J., Casler, J. C., and Glick, B. S. (2018) Budding Yeast Has a Minimal  
1141 Endomembrane System. *Dev Cell* **44**, 56-72
- 1142 67. Graham, T. R., and Burd, C. G. (2011) Coordination of Golgi functions by  
1143 phosphatidylinositol 4-kinases. *Trends Cell Biol* **21**, 113-121
- 1144 68. Bonifacino, J. S., and Glick, B. S. (2004) The mechanisms of vesicle budding  
1145 and fusion. *Cell*. **116**, 153-166
- 1146 69. Buelto, D., Hung, C. W., Aoh, Q. L., Lahiri, S., and Duncan, M. C. (2020)  
1147 Plasma membrane to vacuole traffic induced by glucose starvation requires  
1148 Gga2-dependent sorting at the trans-Golgi network. *Biol Cell* **112**, 349-367
- 1149 70. Casler, J. C., and Glick, B. S. (2020) A microscopy-based kinetic analysis of  
1150 yeast vacuolar protein sorting. *Elife* **25**, e56844
- 1151 71. Hirst, J., Borner, G. H., Antrobus, R., Peden, A. A., Hodson, N. A., Sahlender,  
1152 D. A., and Robinson, M. S. (2012) Distinct and overlapping roles for AP-1 and  
1153 GGAs revealed by the "knocksideways" system. *Curr Biol* **22**, 1711-1716
- 1154 72. Martzoukou, O., Diallinas, G., and Amillis, S. (2018) Secretory Vesicle Polar  
1155 Sorting, Endosome Recycling and Cytoskeleton Organization Require the AP-1  
1156 Complex in *Aspergillus nidulans*. *Genetics* **209**, 1121-1138
- 1157 73. Barlow, L. D., Dacks, J. B., and Wideman, J. (2014) From all to (nearly) none.  
1158 *Cell Logist* **4**, e28114
- 1159 74. Caceres, P. S., Gravotta, D., Zager, P. J., Dephoure, N., and Rodriguez-Boulan,  
1160 E. (2019) Quantitative proteomics of MDCK cells identify unrecognized roles of  
1161 clathrin adaptor AP-1 in polarized distribution of surface proteins. *Proc Natl*  
1162 *Acad Sci USA* **116**, 11796-11805
- 1163 75. Enloe, B., Diamond, A., and Mitchell, A. P. (2000) A single-transformation  
1164 gene function test in diploid *Candida albicans*. *J Bacteriol* **182**, 5730-5736
- 1165 76. Lee, S., Lim, W. A., and Thorn, K. S. (2013) Improved blue, green, and red  
1166 fluorescent protein tagging vectors for *S. cerevisiae*. *PLoS One* **8**, e67902
- 1167 77. Sacristan, C., Manzano-Lopez, J., Reyes, A., Spang, A., Muniz, M., and  
1168 Roncero, C. (2013) Dimerization of the chitin synthase Chs3 is monitored at the  
1169 Golgi and affects its endocytic recycling. *Mol Microbiol* **90**, 252-266
- 1170 78. Arcones, I., Sacristán, C., and Roncero, C. (2016) Maintaining protein  
1171 homeostasis: early and late endosomal dual recycling for the maintenance of  
1172 intracellular pools of the plasma membrane protein Chs3. *Mol Biol Cell* **27**,  
1173 4021-4032

- 1174 79. Gola, S., Martin, R., Walther, A., Dünkler, A., and Wendland, J. (2003) New  
 1175 modules for PCR-based gene targeting in *Candida albicans*: rapid and efficient  
 1176 gene targeting using 100 bp of flanking homology region. *Yeast* **20**, 1339-1347  
 1177 80. Schaub, Y., Dünkler, A., Walther, A., and Wendland, J. (2006) New pFA-  
 1178 cassettes for PCR-based gene manipulation in *Candida albicans*. *J Basic*  
 1179 *Microbiol* **46**, 416-429

1180  
 1181

1182 **TABLES**

1183

1184 **Table 1. Yeast strains used.**

1185

1186

1187 Strain	1187 Genotype	1187 Origin / Reference
-------------	---------------	-------------------------

1188

1189 **S. cerevisiae strains**

1190 CRM67	1190 W303, mat a, 1191 ( <i>leu2-3,112 trp1-1 can1-100 ura3-1 ade2-1 his3-11,15</i> )	1191 Lab. collection
1192 CRM2268	1192 W303, mat a, <i>chs5Δ::natMx4</i>	1192 Lab. Collection
1193 CRM3066	1193 W303, mat a, <i>bch1Δ::kanMx4 bud7Δ::natMx4</i>	1193 (42)
1194 CRM3081	1194 W303, mat a, <i>chs6Δ::kanMx4 bch2Δ::natMx4</i>	1194 (42)
1195 CRM3851	1195 W303, mat a, <i>tat2Δ::hphNT1</i>	1195 This study
1196 CRM3853	1196 W303, mat a, <i>chs5Δ::natMx4 tat2Δ::hphNT1</i>	1196 This study
1197 CRM3909	1197 W303, mat a, PGAL1- <i>TAT2::KanMx4</i>	1197 This study
1198 CRM3917	1198 W303, mat a, <i>chs5Δ::natMx4 PGAL1-TAT2::KanMx4</i>	1198 This study
1199 CRM2868	1199 W303, mat a, PGAL1- <i>GFP-SSY1::KanMx4</i>	1199 This study
1200 CRM2871	1200 W303, mat a, <i>chs5Δ::natMx4 PGAL1-GFP-SSY1::KanMx4</i>	1200 This study
1201 CRM3811	1201 W303, mat a, <i>STP1-3xHA::hphNT1</i>	1201 This study
1202 CRM3825	1202 W303, mat a, <i>STP1-3xHA::hphNT1 chs5Δ::natMx4</i>	1202 This study
1203 CRM3813	1203 W303, mat a, <i>GLN3-3xHA::hphNT1</i>	1203 This study
1204 CRM3827	1204 W303, mat a, <i>GLN3-3XHA::hphNT1 chs5Δ::natMx4</i>	1204 This study
1205 CRM3023	1205 W303, mat a, <i>GTR1-GFP::hphNT1</i>	1205 This study
1206 CRM3032	1206 W303, mat a, <i>chs5Δ::natMx4 GTR1-GFP::hphNT1</i>	1206 This study
1207 CRM3017	1207 W303, mat a, <i>TCO89-GFP::hphNT1</i>	1207 This study
1208 CRM3020	1208 W303, mat a, <i>chs5Δ::natMx4 TCO89-GFP::hphNT1</i>	1208 This study

1209	CRM2972	W303, mat a, <i>GAP1-GFP::hphNT1</i>	This study
1210	CRM2979	W303, mat a, <i>chs5Δ::natMx4 GAP1-GFP::hphNT1</i>	This study
1211	CRM2894	W303, mat a, <i>TAT2-GFP::hphNT1</i>	This study
1212	CRM2903	W303, mat a, <i>chs5Δ::natMx4 TAT2-GFP::hphNT1</i>	This study
1213	CRM3531	W303, mat a, <i>MUPI-GFP::KanMx4</i>	This study
1214	CRM3540	W303, mat a, <i>MUPI-GFP::KanMx4 chs5Δ::natMx4</i>	This study
1215	CRM3882	W303, mat a, <i>TAT2<sup>52-53</sup>-3xHA</i> (internal by <i>Delitto Perfetto</i> )	This study
1216	CRM3890	W303, mat a, <i>TAT2<sup>52-53</sup>-3xHA chs5Δ::kanMx4</i>	This study
1217	CRM3862	W303, mat a, <i>bul1Δ::kanMx4</i>	This study
1218	CRM3903	W303, mat a, <i>bul2Δ::hphNT1</i>	This study
1219	CRM3880	W303, mat a, <i>bul1Δ::kanMx4 bul2Δ::hphNT1</i>	This study
1220	CRM3864	W303, mat a, <i>chs5Δ::kanMx4 bul1Δ::kanMx4</i>	This study
1221	CRM3915	W303, mat a, <i>bul2Δ::hphNT1 chs5Δ::natMx4</i>	This study
1222	CRM3888	W303, mat a, <i>bul1Δ::kanMx4 bul2Δ::hphNT1 chs5Δ::natMx4</i>	This study
1223	CRM1700	W303, mat a, <i>rcy1Δ::kanMx4</i>	Lab. Collection
1224	CRM2160	W303, mat a, <i>rcy1Δ::kanMx4 chs5Δ::natMx4</i>	Lab. Collection
1225	CRM3155	W303, mat a, <i>aps1Δ::kanMx4</i>	This study
1226	CRM3157	W303, mat a, <i>chs5Δ::natMx4 aps1Δ::kanMx4</i>	This study
1227	CRM3520	W303, mat a, <i>gga1Δ::natMx4</i>	Lab. Collection
1228	CRM3523	W303, mat a, <i>gga2Δ::hphNT1</i>	Lab. Collection
1229	CRM3621	W303, mat a, <i>gga2Δ::hphNT1 gga1Δ::natMx4</i>	Lab. Collection
1230	CRM3905	W303, mat a, <i>gga2Δ::hphNT1 gga1Δ::natMx4 chs5Δ::kanMx4</i>	This study
1231	CRM3949	W303, mat a, <i>gga1Δ::natMx4 chs5Δ::kanMx4</i>	This study
1232	CRM3950	W303, mat a, <i>gga2Δ::hphNT1 chs5Δ::kanMx4</i>	This study
1233	CRM3526	W303, mat a, <i>rcy1Δ::kanMx4 gga1Δ::natMx4</i>	Lab. Collection
1234	CRM3602	W303, mat a, <i>rcy1Δ::kanMx4 gga2Δ::hphNT1</i>	Lab. Collection
1235	CRM4025	W303, mat a, <i>rcy1Δ::kanMx4 aps1Δ::hphNT1</i>	This study
1236	CRM3432	W303, mat a, <i>APL4-VC::kanMx4 CHS5-VN::HIS3</i>	This study
1237	CRM3477	W303, mat a, <i>CHS5-VC::kanMx4</i>	This study
1238	CRM3997	W303, mat a, <i>CHS5-VN::kanMx4</i>	This study
1239	CRM4003	W303, mat a, <i>CHS5-VN::kanMx4 MUPI-VC::HIS3</i>	This study
1240	CRM4070	W303, mat a, <i>CHS5-VN::kanMx4 GGA2-VC::HIS3</i>	This study
1241	CRM2879	W303, mat a, <i>SEC7-mRuby2::kanMx4</i>	This study
1242	CRM2882	W303, mat a, <i>chs5Δ::natMx4 SEC7-mRuby2::kanMx4</i>	This study
1243	CRM4088	W303, mat a, <i>arf1Δ::kanMx4</i>	This study
1244	CRM4090	W303, mat a, <i>chs5Δ::natMx4 arf1Δ::kanMx4</i>	This study
1245	CRM1278	W303, mat a, <i>chs3Δ::URA3 chs5Δ::natMx4</i>	Lab. Collection

1246	CRM1590	W303, mat a, <i>chs3Δ::natMx4</i>	Lab. Collection
1247	CRM3089	W303, mat a, <i>bch1Δ::kanMx4 bud7Δ::natMx4 chs3Δ::hphNT1</i>	This study
1248	CRM3091	W303, mat a, <i>chs6Δ::kanMx4 bch2Δ::natMx4 chs3Δ::hphNT1</i>	This study
1249	CRM4098	W303, mat a, <i>chs3Δ::URA3 chs6Δ::kanMx4</i>	This study
1250	CRM3534	W303, mat a, <i>CHS5-VC::kanMx4 gga2Δ::hphNT1</i>	This study
1251	CRM3511	W303, mat a, <i>CHS5-VC::kanMx4 chs6Δ::natMx4 bch2Δ::hphNT1</i>	This study
1252	CRM3668	W303, mat a, <i>CHS5-VC::kanMx4 bch1Δ::hphNT1 bud7Δ::natMx4</i>	This study
1253	CRM3641	W303, mat a, <i>CHS5-VC::kanMx4 chs7Δ::hphNT1</i>	This study
1254	CRM3674	W303, mat a, <i>CHS5-VC::kanMx4 chs3Δ::URA3</i>	This study
1255	CRM3511	W303, mat a, <i>CHS5-VC::kanMx4 chs6Δ::natMx4</i>	This study
1256	CRM3676	W303, mat a, <i>CHS5-VC::kanMx4 chs6Δ::natMx4 chs3Δ::URA3</i>	This study
1257	CRM3432	W303, mat a, <i>APL4-VC::kanMx4</i>	This study
1258	CRM3453	W303, mat a, <i>APL4-VC::kanMx4 gga2Δ::hphNT1</i>	This study
1259	CRM3436	W303, mat a, <i>chs3Δ::URA3 APL4-VC::kanMx4</i>	This study
1260	CRM2248	W303, mat a, <i>CHS5-mCherry::natMx4 APS1-GFP::hphNT1</i>	Lab. Collection
1261	CRM2533	W303, mat a, <i>CHS5-mCherry::natMx4 GGA1-GFP::hphNT1</i>	Lab. Collection
1262	CRM808	BY4741, mat a ( <i>his3Δ1, leu2Δ0, met15Δ0, ura3Δ0</i> )	EUROSCARF
1263	CRM1435	BY4741, mat a, <i>chs3Δ::natMx4</i>	Lab. Collection
1264	CRM2453	BY4741, mat a, <i>chs3Δ::natMx4 chs5Δ::hphNT1</i>	Lab. Collection
1265	CRM3922	BY4741, mat a, <i>chs5Δ::natMx4</i>	Lab. Collection
1266	CRM3924	BY4741, mat a, <i>art1Δ::kanMx4 chs5Δ::natMx4</i>	This study
1267	CRM3926	BY4741, mat a, <i>art2Δ::kanMx4 chs5Δ::natMx4</i>	This study
1268	CRM3928	BY4741, mat a, <i>art3Δ::kanMx4 chs5Δ::natMx4</i>	This study
1269	CRM3930	BY4741, mat a, <i>art4Δ::kanMx4 chs5Δ::natMx4</i>	This study
1270	CRM3932	BY4741, mat a, <i>art5Δ::kanMx4 chs5Δ::natMx4</i>	This study
1271	CRM3934	BY4741, mat a, <i>art6Δ::kanMx4 chs5Δ::natMx4</i>	This study
1272	CRM3935	BY4741, mat a, <i>art7Δ::kanMx4 chs5Δ::natMx4</i>	This study
1273	CRM3937	BY4741, mat a, <i>art8Δ::kanMx4 chs5Δ::natMx4</i>	This study
1274	CRM3939	BY4741, mat a, <i>art9Δ::kanMx4 chs5Δ::natMx4</i>	This study
1275	CRM3941	BY4741, mat a, <i>art10Δ::kanMx4 chs5Δ::natMx4</i>	This study
1276	CRM4019	BY4741, mat a, <i>GGA2-GFP::hphNT1 APL4-mCherry::natMx4</i>	This study
1277	CRM2761	X2180-1A, mat a ( <i>SUC2 mal mel gal2 CUP1</i> )	Francisco del Rey
1278	CRM2763	X2180-1A, mat a, <i>chs5Δ::kanMx4</i>	This study
1279	CRM3957	X2180-1A, mat a, <i>tat2Δ::kanMx4</i>	This study
1280	CRM3959	X2180-1A, mat a, <i>chs5Δ::kanMx4 tat2Δ::kanMx4</i>	This study
1281	CRM2783	X2180-1A, mat a, <i>ssy1Δ::natMx4</i>	This study
1282	CRM3010	X2180-1A, mat a, <i>ssy1Δ::natMx4 chs5Δ::kanMx4</i>	This study

1283	CRM4311	W303, mat a, <i>ARF1-GFP::hphNT1</i>	This study
1284	CRM4134	W303, mat a, <i>CHS3-2xGFP::hphNT1</i>	This study
1285	CRM4136	W303, mat a, <i>CHS3-2xGFP::hphNT1 chs5Δ::natMx4</i>	This study
1286	CRM4140	W303, mat a, <i>CHS3-2xGFP::hphNT1 arf1Δ::kanMx4</i>	This study
1287	CRM4138	W303, mat a, <i>CHS3-2xGFP::hphNT1 chs5Δ::natMx4</i>	
1288		<i>arf1Δ::kanMx4</i>	This study
1289	CRM4157	W303, mat a, <i>PGAL1-ARF1::KanMx4</i>	This study
1290	CRM4159	W303, mat a, <i>chs5Δ::natMx4 PGAL1-ARF1::KanMx4</i>	This study
1291	CRM4302	W303, mat a, <i>PGAL1-SEC7::KanMx4</i>	This study
1292	CRM4339	W303, mat a, <i>PGAL1-SEC7::KanMx4 chs5Δ::natMx4</i>	This study
1293	CRM2818	BY4741, mat a, <i>CHS5-GFP::hphNT1</i>	Lab. Collection
1294	CRM4160	BY4741, mat a, <i>CHS5-GFP::hphNT1 arf1Δ::kanMx4</i>	This study
1295	CRM4594	W303, mat a, <i>CHS5-VN::kanMx4 ANP1-VC::HIS3</i>	This study
1296	CRM4586	W303, mat a, <i>CHS5-mCherry::natMx4 GGA1-GFP::hphNT1</i>	
1297		<i>arf1Δ::kanMx4</i>	This study
1298	CRM4584	W303, mat a, <i>CHS5-GFP::hphNT1</i>	This study
1299	CRM4573	W303, mat a, <i>PGAL1-GGA2::KanMx4 CHS5-GFP::hphNT1</i>	This study
1300	CRM4118	W303, mat a, <i>APSI-GFP::hphNT1</i>	This study
1301	CRM4153	W303, mat a, <i>PGAL1-GGA2::KanMx4 APSI-GFP::hphNT1</i>	This study
1302	CRM4571	W303, mat a, <i>PGAL1-BUD7::KanMx4 APSI-GFP::hphNT1</i>	This study
1303	CRM4576	W303, mat a, <i>PGAL1-BCH1::KanMx4 APSI-GFP::hphNT1</i>	This study
1304			
1305		<b><u>C. albicans strains</u></b>	
1306	CRM2499	BWP17, ( <i>ura3::imm434/ura3::imm434 his1::hisG/his1::hisG</i>	
1307		<i>arg4::hisG/arg4::hisG</i> )	(75)
1308	CRM2531	BWP17, <i>Cachs5Δ::ARG4/Cachs5Δ::HIS1</i>	Lab. Collection
1309	CRM3258	BWP17, <i>Caaps1Δ::SAT1/Caaps1Δ::URA3</i>	This study
1310	CRM3261	BWP17, <i>Cachs5Δ::ARG4/Cachs5Δ::HIS1</i>	
1311		<i>Caaps1Δ::SAT1/Caaps1Δ::URA3</i>	This study
1312			
1313			
1314			
1315			
1316			
1317			

1318

1319 **Table 2. Plasmids used.**

1320

1321

1322	Plasmid	Genotype	Origin / Reference
1323			
1324			
1325	CRM160	pRS313 ( <i>HIS3</i> )	Lab collection
1326	CRM161	pRS314 ( <i>TRP1</i> )	Lab collection
1327	CRM264	pRS315 ( <i>LEU2</i> )	Lab collection
1328	CRM265	pRS316 ( <i>URA3</i> )	Lab collection
1329	CRM166	pRS426 ( <i>URA3</i> )	Lab collection
1330	CRM2546	pAG25 ( <i>natMx4</i> )	(32)
1331	CRM1188	pUG6 ( <i>kanMx4</i> )	(32)
1332	CRM2546	pUG72 ( <i>URA3</i> )	(32)
1333	CRM1451	pFA6a- <i>hphNT1</i>	(32)
1334	CRM1807	pFA6a-3xHA:: <i>hphNT1</i>	(34)
1335	CRM1995	pFA6a-GFP:: <i>hphNT1</i>	(34)
1336	CRM1811	pFA6a-GFP:: <i>natMx4</i>	(34)
1337	CRM2653	pFN21 ( <i>mCherry</i> :: <i>natMx4</i> )	(34)
1338	CRM2037	pFA6a- <i>kanMX4</i> -pGAL1	(33)
1339	CRM2827	pFA6a- <i>kanMX4</i> -pGAL1-GFP	(33)
1340	CRM2360	pGSHU (CORE Delitto Perfetto)	(35)
1341	CRM3469	pFA6a- <i>VenusCterminal</i> :: <i>HIS3</i>	(39)
1342	CRM3470	pFA6a- <i>VenusNterminal</i> :: <i>HIS3</i>	(39)
1343	CRM3471	pFA6a- <i>VenusCterminal</i> :: <i>kanMX4</i>	(39)
1344	CRM3472	pFA6a- <i>VenusNterminal</i> :: <i>kanMX4</i>	(39)
1345	CRM2328	pFA6a- link- <i>yomRuby2</i> :: <i>CaURA3</i>	(76)
1346	CRM1131	pRS315:: <i>CHS3-GFP</i>	(77)
1347	CRM3456	pRS315:: <i>CHS3-VN</i> :: <i>HIS3</i>	This study
1348	CRM2084	pRS315:: <i>CHS3<sup>L24A</sup>-GFP</i>	(78)
1349	CRM1868	pRS315-GFP-Snc1	Anne Spang
1350	CRM3236	pFA- <i>CaHIS1</i>	(79)
1351	CRM3238	pFA- <i>CaARG4</i>	(79)
1352	CRM3240	pFA- <i>CaURA3</i>	(79)



1354

1355

1356

1357

1358

1359

1360 **Table 3. ImageJ Macros used:**

1361

1362

1363 **Macro1: Pre-filtering for dot co-localization**

1364

1365

1366 showMessage("Open Channel Red"); //Select Channel Red

1367 open();

1368 red = getTitle();

1369 showMessage("Open Channel GFP"); //Select Channel GFP

1370 open();

1371 gfp = getTitle(); //Then, we are going to filter both channels

1372 selectWindow(gfp);

1373 run("Median...", "radius=1 stack"); //Filtering

1374 run("Unsharp Mask...", "radius=2 mask=0.5 stack"); //Filtering

1375 selectWindow(red);

1376 run("Median...", "radius=1 stack"); //Filtering

1377 run("Unsharp Mask...", "radius=2 mask=0.5 stack"); //Filtering

1378 run("JACoP "); //Open JACoP plugin

1379

1380

1381

1382 **Macro2: Analyze dots**

1383

1384

1385 showMessage("Open the Image"); //Select image

1386 open();

1387 run("Duplicate...", ""); //We want to do the segmentation in a copy of the original, therefore we duplicate

1388 run("Median...", "radius=1"); //Filtering

1389 run("Unsharp Mask...", "radius=2 mask=0.50"); //Filtering

1390 run("Threshold..."); // to open the threshold window if not opened yet

1391 waitForUser("Set the threshold and press OK, or cancel to exit macro"); // pauses the execution and lets you access ImageJ

1392 manually

```

1393 run("Analyze Particles..."); //to take the ROIs
1394 waitForUser("Finally, use these ROIs in the original window"); //A note to correctly continue after the macro
1395
1396
1397
1398 Macro3: Counting colonies
1399
1400
1401 showMessage("Open the Image"); //Select image with colonies
1402 open();
1403 rename("Initial");
1404 run("Duplicate...", "");
1405 run("Threshold..."); // to open the threshold window if not opened yet
1406 waitForUser("set the threshold and press OK, or cancel to exit macro");
1407 // pauses the execution and lets you access ImageJ manually as long as you don't press OK, which resumes the macro execution
1408 run("Convert to Mask"); // to binarize, if you use this command, don't press 'Apply' in the threshold window
1409 run("Watershed"); //to separate close colonies
1410 rename("Mask");
1411 waitForUser("Calibration: Draw a line along the Petri dish \nand introduce the known size in Analyze/SetScale, then press OK");
1412 run("Threshold...");
1413 waitForUser("Set the threshold and press OK, or cancel to exit macro"); // pauses the execution and lets you access ImageJ
1414 manually
1415 run("Analyze Particles..."); //to take the ROIs

```

1416  
1417  
1418  
1419

## 1420 **FIGURE LEGENDS**

1421

1422 **Figure 1.** Ammonium sensitivity of the exomer mutants is due to defects in amino acid  
1423 uptake. (A) Overnight (O/N) cultures of the indicated strains in the W303 genetic  
1424 background were diluted and plated onto YEPD media supplemented with 0.2 M  
1425 NH<sub>4</sub>Cl. Note the similar level of sensitivity of the *chs5*Δ and *bch1*Δ/*bud7*Δ mutants. (B)  
1426 O/N cultures of the indicated strains in the W303 background were diluted and spread  
1427 on synthetic defined media (SD) supplemented with the indicated concentrations of  
1428 tryptophan. Note that low concentrations (%) of tryptophan (Trp) allowed the wild-type  
1429 strain to completely grow, but was unable to efficiently support the growth of the *chs5*Δ  
1430 mutant. The numbers indicate the average diameter ± standard deviation of the colonies  
1431 growing on the different media quantified using *ImageJ* (Macro3). Also refer to

1432 supplemental Figure S1 for additional data on ammonium sensitivity. (C) L-[5-<sup>3</sup>H]-  
1433 tryptophan uptake in SD media by the indicated X2180-derived prototrophic strains.  
1434 Numeric values indicate the incorporation rate (dpm/A<sub>600</sub>/min) calculated as the slope of  
1435 the linear regression made using 10 to 40 minutes time points. Note the absence of Trp  
1436 incorporation in the *tat2Δ* mutants used as the control. (D) Sensitivity of the indicated  
1437 X2180-derived strains to toxic amino acids analogs. Growth was analyzed in YEPD  
1438 supplemented with the indicated concentrations of the following analogs: Sulfometuron-  
1439 metil; L-canavanine; L-azetidin-2-carboxilate (AzC); 3-aminotriazole (3-AT) and L-  
1440 histidine as indicated. (E) Western blot of the total protein from the cellular extracts of  
1441 strains carrying *STP1*-3xHA integrated at the chromosomal locus. Cultures starved for 1  
1442 hour in YNB-N-aa media were transferred to rich YEPD media and samples were taken  
1443 at 0 and 30 minutes. Note the similar processing of the Spt1 transcription factor in the  
1444 wild-type and *chs5Δ* strains. (F) Induction of Rsp6 phosphorylation after adding  
1445 glutamine. X2180 strains grown on SD complete media were transferred to media  
1446 lacking a nitrogen source for 1h; glutamine (500 μg/ml) was then added to the media.  
1447 Note that the kinetics of the phosphorylation induced in the wild type and *chs5Δ* are  
1448 similar. Phosphorylation was determined by Western blot using a phospho-(Ser/Thr)  
1449 Akt substrate antibody (#9611s, Cell SignalingTech). Also refer to supplemental Figure  
1450 S2 for the rationale behind these experiments.

1451

1452 **Figure 2.** Exomer controls the traffic of several amino acid permeases. (A) Localization  
1453 of Tat2-GFP and Mup1-GFP under steady state growth conditions in induction media.  
1454 Note the subtle differences of Tat2 and Mup1 intracellular localization in the exomer  
1455 mutant and their accumulation at intracellular spots (see arrowheads). (B) Intracellular  
1456 distribution of Tat2<sup>52-53</sup>-3xHA in wild-type and *chs5Δ* strains after discontinuous  
1457 subcellular fractionation. Proteins were visualized by Western blot as described in the  
1458 Material and Methods section. Graphs on the right represent the percentage of each  
1459 protein at each fraction. Pma1 and Pep12 were used as markers for the PM and  
1460 TGN/endosome fraction respectively. (C) Analysis of the PM anterograde transport of  
1461 Tat2-GFP and Mup1-GFP, with their gene expression under the control of the GAL1  
1462 promoter. In both cases, for pGAL-*TAT2*-GFP and pGAL-*MUPI*-GFP strains, the cells  
1463 were grown O/N in SD 2 % raffinose media and then transferred to a SD 2% galactose  
1464 media. In the case of Tat2, and taking in to account the lethality of the lack of Tat2,  
1465 0.02% Trp was added to the SD raffinose media and the galactose induction phase was

1466 done in a SD media with standard tryptophan concentrations (0.002 %). All images  
1467 were acquired just one hour after the addition of galactose. (D) Quantitative analysis of  
1468 the polarization of these proteins along the PM using images from the experiment  
1469 shown in C. A daughter cell/ mother cell PM signal coefficient was measured following  
1470 the scheme shown in the left panel (details in Material and Methods section). The  
1471 horizontal dashed line represents the condition of the lack of polarization of PM protein  
1472 distribution. (E) Localization and dynamics of Tat2-GFP after the induction of its  
1473 endocytosis in Trp-depleted media (53). The same experiment was analyzed by Western  
1474 blot and relative protein degradation after 60 min of induction was calculated from 3  
1475 independent experiments (lower panels). (F) Localization and dynamics of Mup1-GFP  
1476 after the induction of its endocytosis by adding methionine (20 mg/L) (54). The same  
1477 experiment was analyzed by Western blot and relative protein levels were calculated for  
1478 each point (lower panel).

1479

1480 **Figure 3.** The need for tryptophan and the blockage of chitin synthesis of the *chs5Δ*  
1481 mutant are differentially suppressed by several mutations affecting TGN traffic. (A)  
1482 Growth of the indicated strains in YEPD media with the indicated supplements. (B)  
1483 Growth of the indicated strains in SD w/o Trp media supplemented with the indicated  
1484 concentrations of Trp. (C, D) Growth of the indicated strains in YEPD media with the  
1485 indicated supplements. All strains used are W303 derivatives grown O/N in YEPD  
1486 media, serially diluted and plated onto the indicated media. Each panel represents a  
1487 single experiment using a unique set of plates; note the slight differences in the growth  
1488 of similar strains between different panels/experiments. (E) Calcofluor staining of the  
1489 indicated strains. Cells grown in YEPD media were stained for 1.5 hours with  
1490 calcofluor (50 μg/ml). Note the reduction in calcofluor staining shown by all *chs5Δ*  
1491 strains that is partially reverted by *gga2Δ*, *gga1Δ/gga2Δ* and *aps1Δ* concomitant  
1492 mutations. This result coincides with their higher level of sensitivity to this drug, which  
1493 is shown in the other figure panels.

1494

1495 **Figure 4.** Exomer contributes to TGN clathrin adaptor recruitment. (A) BIFC analysis  
1496 of the interaction of Chs5-VN with the indicated proteins tagged with the VC fragment.  
1497 Note the unexpected localization of Chs5-VN/Chs3-VC along the PM. (B) Time-lapse  
1498 analysis of the recruitment of the clathrin adaptor complexes and exomer. Individual  
1499 dots for each protein were visualized by two color confocal spinning disk microscopy

1500 over time. Graphs represent the average recruitment duration of each complex using  
1501 exomer as a reference. For more detailed information see Figure S5. (C) Localization of  
1502 Apl4-mCh and Gga2-GFP in the wild-type and *chs5Δ* strains. Note the larger and more  
1503 intense dots of both proteins in *chs5Δ* and the apparent increase in co-localization. (D)  
1504 Quantitative analysis of Gga2-GFP and Apl4-mCh dots in the experiment shown in C.  
1505 Note the significant increase in the area and intensity of the dots for both proteins in the  
1506 absence of exomer. The results are the average of 4 independent experiments. (E) Co-  
1507 localization analysis between Gga2-GFP and Apl4-mCh. The values are the average of  
1508 four independent experiments. (F) Sensitivity of the indicated strains to myriocin and  
1509 sertraline represented by the IC50 coefficient, calculated as described in the Material  
1510 and Method section. Values represent the average of six independent experiments.

1511

1512 **Figure 5.** Functional link between Arf1 GTPase and the exomer complex. (A)  
1513 Localization of Sec7-mR2 in the wild-type and *chs5Δ* strains. The right panels show the  
1514 quantitative analysis of Sec7-mR2 TGN structures using Macro2. The box-plots  
1515 represent the intensity and the area of Sec7-mR2 dots (the average is represented by the  
1516 dashed line,  $n \geq 700$  dots acquired in 4 independent experiments). (B) Analysis of Sec7-  
1517 mR2 dynamics in the absence of exomer with the *TrackMate* ImageJ plugin. The Box-  
1518 plots represent the average track displacement of Sec7-mR2 dots calculated from more  
1519 than 2500 trajectories for each strain acquired in 4 independent experiments (the  
1520 average is represented by the dashed line). See Figure S6C for additional data on the  
1521 dynamics of Sec7. (C) Effect of Arf1 deletion on chitin synthesis. Upper panels show  
1522 calcofluor staining in the indicated strains. Lower panels show the localization of Chs3-  
1523 2xGFP in the indicated strains. Arrows show the accumulation of Chs3 at bud necks  
1524 and the arrowheads mark aberrant TGN/EE structures. (D) Effects of the deregulation of  
1525 Arf1/Sec7 expression in cells expressing the indicated chromosomal genes from the  
1526 GAL1 promoter in the wild-type or *chs5Δ* strains. Cells were grown O/N in YEP 2 %  
1527 raffinose and 0.1 % galactose, serially diluted and spotted on the indicated media  
1528 containing glucose (upper panel) or galactose (lower panel) as the carbon source.  
1529 Growth was recorded after 2-3 days at 28°C. Note how the pGAL1-*SEC7* strains were  
1530 unable to grow on media containing glucose. (E) Calcofluor staining of multiple strains  
1531 in which the indicated chromosomal gene is under the control of the GAL1 promoter.  
1532 Cells were grown O/N as indicated above and transferred to the indicated media for two  
1533 hours; then, calcofluor was added and chitin staining was visualized after an additional

1534 90 minutes. Note that repression of *ARF1* and *SEC7* in glucose media restored  
1535 calcofluor staining in the *chs5Δ* mutant.

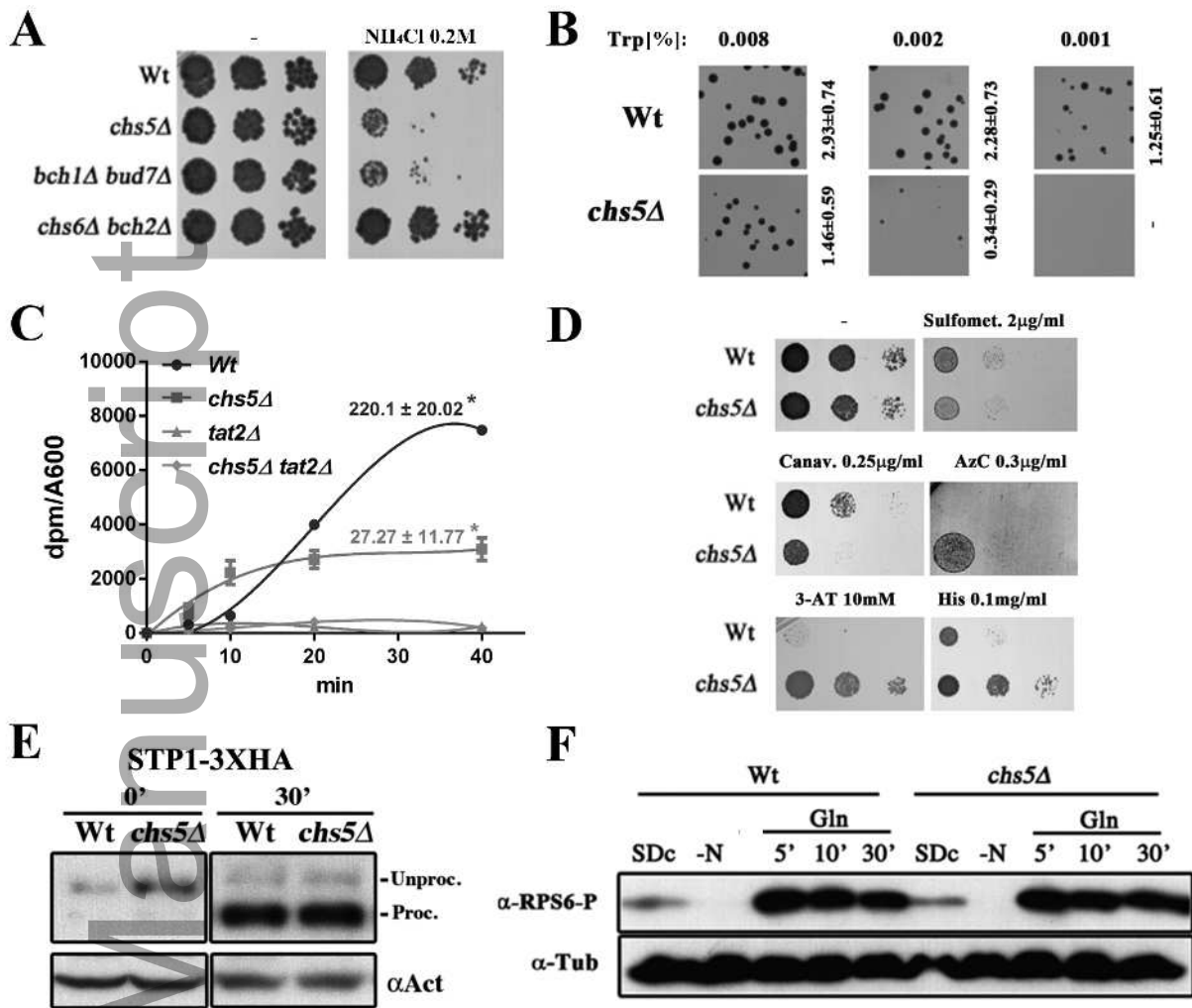
1536

1537 **Figure 6.** Analysis of Chs3 transport reveals different phenotypes among the mutants of  
1538 different exomer subunits and shows cargo competition between the exomer and AP-1  
1539 complexes. (A) Localization of Chs3-GFP in *chs5Δ* and *chs6Δ bch2Δ* mutants. Static  
1540 images and quantitative analysis of the intracellular dots of Chs3 in both mutants are  
1541 shown. Note the reduced diameter and intensity of Chs3-GFP in the *chs6Δ bch2Δ* strain  
1542 compared to *chs5Δ*. (B) Calcofluor sensitivity of cells expressing wild-type Chs3 and  
1543 mutant <sup>L24A</sup>Chs3 proteins. (C) Analysis of the Chs3/Chs5 interaction by BIFC. Most of  
1544 the signal is distributed along the PM, even in the absence of a functional exomer as in  
1545 the *bud7Δ bch1Δ* double mutant. However, this localization is prevented if Chs3 exit  
1546 from the ER is blocked as in the *chs7Δ* mutant. (D) Calcofluor resistance of the  
1547 different Chs3 constructs in the indicated strains. Note that the interaction Chs5-  
1548 VC/Chs3-VN suppressed the resistance of the *chs6Δ* mutant to calcofluor, similar to the  
1549 effects observed for the <sup>L24A</sup>Chs3 protein. (E) Analysis of the Chs3/Apl4 interaction by  
1550 BIFC. Upper panel shows localization of Chs3/Apl4 interaction. Lower panel shows  
1551 calcofluor resistance of the indicated strains. Note that Apl4-VC/Chs3-VN interaction  
1552 confers moderate resistance to calcofluor on its own (lower panel).

1553

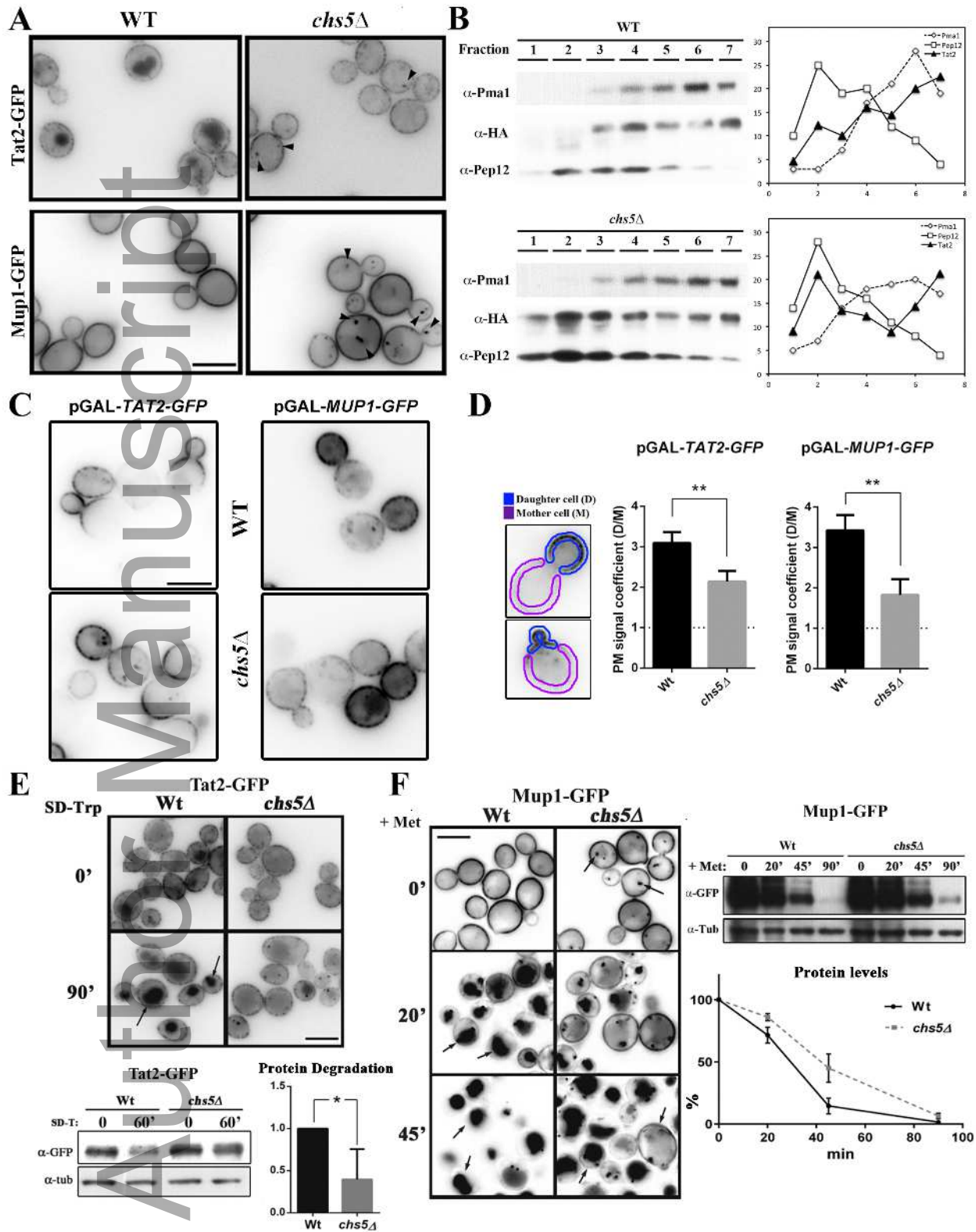
1554 **Figure 7.** Exomer and clathrin adaptors in protein sorting: implications of exomer and  
1555 AP-1 relationship in *Candida albicans* physiology and a model for TGN sorting. (A) *C.*  
1556 *albicans* cells of the indicated strains were induced for filamentation at 37°C in  
1557 filamentation media (YEPD, 80 mg/L uridine and 10 % fetal bovine serum). Images  
1558 were acquired after 2 hours of growth. (B) Quantification of the length of the hyphae in  
1559 the experiment shown in A. (C) *C. albicans* filamentation in different solid media.  
1560 Individual cells were plated onto the indicated filamentation media and incubated for 3-  
1561 4 days at 37°C. Images were acquired with a stereomicroscope with upper (left panel) or  
1562 lower (central and right panels) illumination. Right panels present images with a higher  
1563 amplification to show the details of filamentation (scales 1cm and 2mm). Note the  
1564 absence of hyphae in the *aps1Δ* and *aps1Δ chs5Δ* mutants under all conditions tested.  
1565 All tested strains are diploids and homozygous for the indicated genes. (D) Exomer and  
1566 CCV are assembled at nearby localizations of the TGN and share a requirement for  
1567 Arf1-GTPase activity. Exomer assembles as different complexes with different

1568 properties and facilitates the anterograde delivery of multiple proteins to the PM. CCV  
1569 vesicles facilitate the late endosomal traffic of several proteins, affecting their recycling.  
1570 (E) Exomer is required for the transport to the PM of a limited set of proteins that  
1571 interact with both the exomer and AP-1 complexes (red lines). The anterograde traffic  
1572 and the recycling of these *bona fide* exomer cargoes strictly depend on the coordinated  
1573 action of both exomer and AP-1, a distinctive characteristic of *S. cerevisiae* cells. By  
1574 contrast, exomer has a more general role in protein sorting at the TGN region that  
1575 facilitates polarized delivery of multiple proteins to the PM, independent of Rcy1-  
1576 mediated recycling (green lines). In addition, exomer contributes to the correct  
1577 assembly of the clathrin adaptor complexes, thereby, facilitating the proper late  
1578 endosomal traffic of multiple proteins through the vacuole. Disruption of these clathrin  
1579 adaptor complexes allows the transit of all these proteins to the PM by alternative  
1580 pathways. PM: plasma membrane, TGN: trans-Golgi network; MVB: multi vesicular  
1581 body. (F) A diagram showing the differential role of the exomer and AP-1 complexes in  
1582 the polarized growth of fungi depending on how cells grow as yeasts or as hyphae.

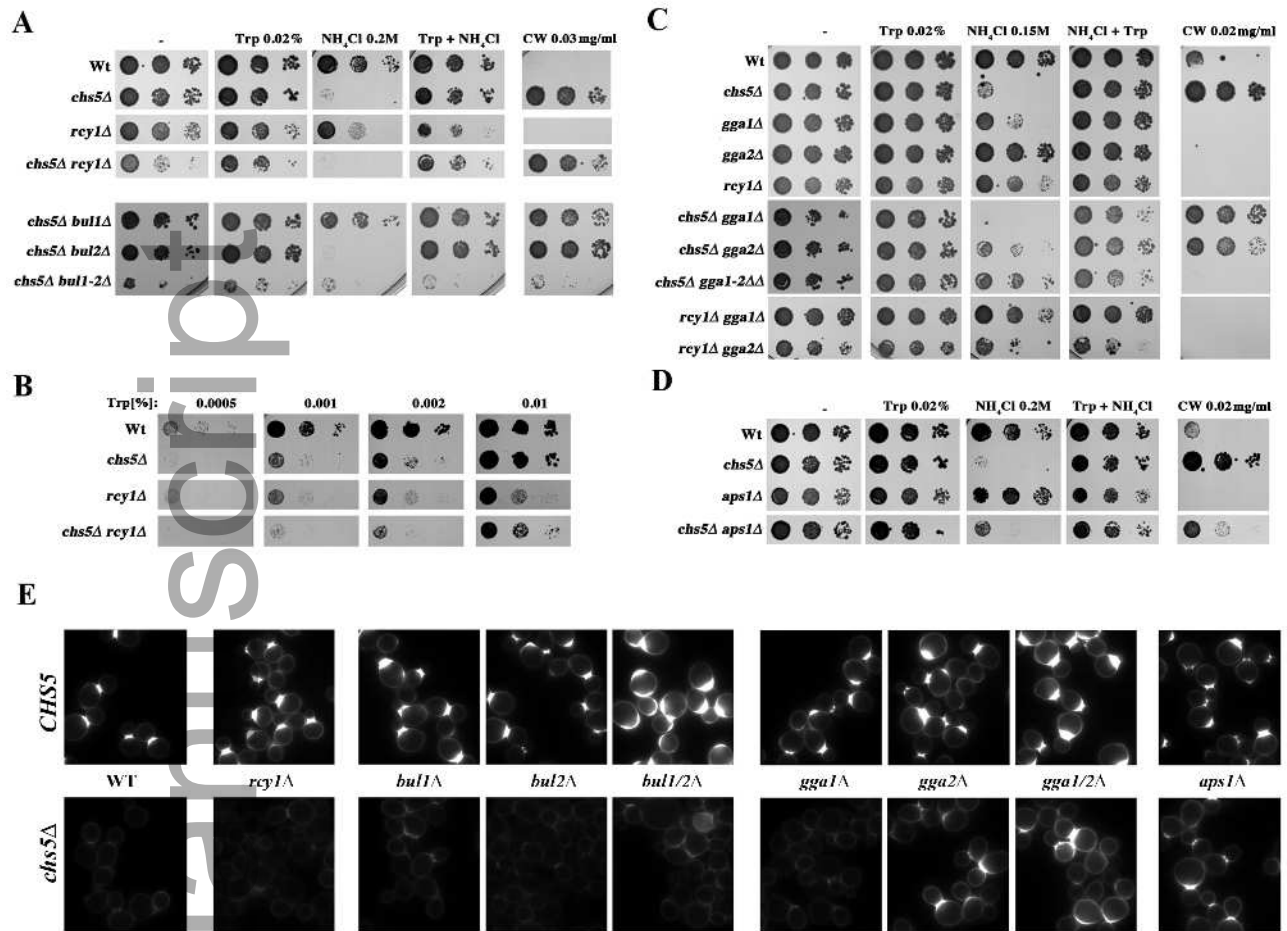


fsb2\_21615\_f1.tif

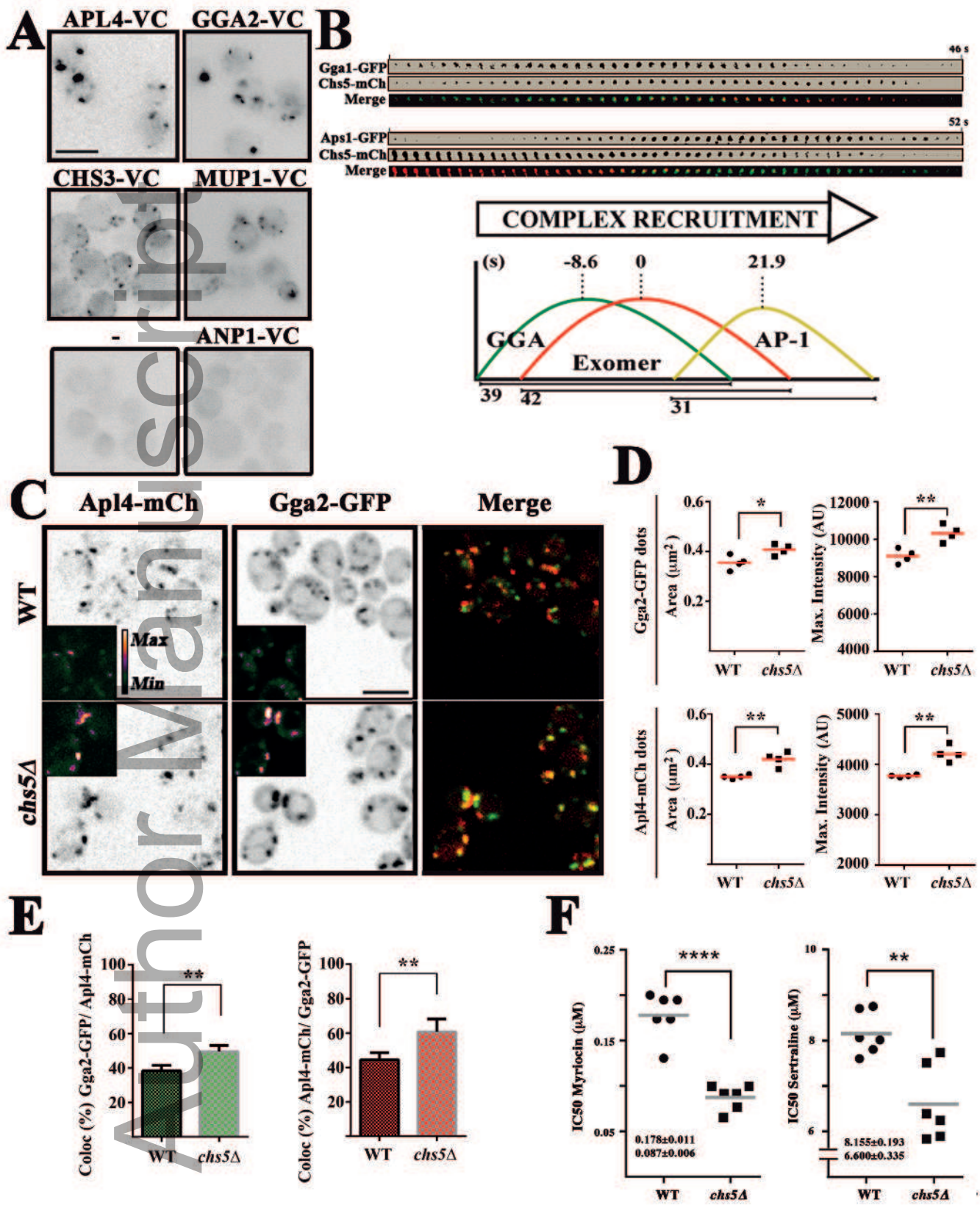




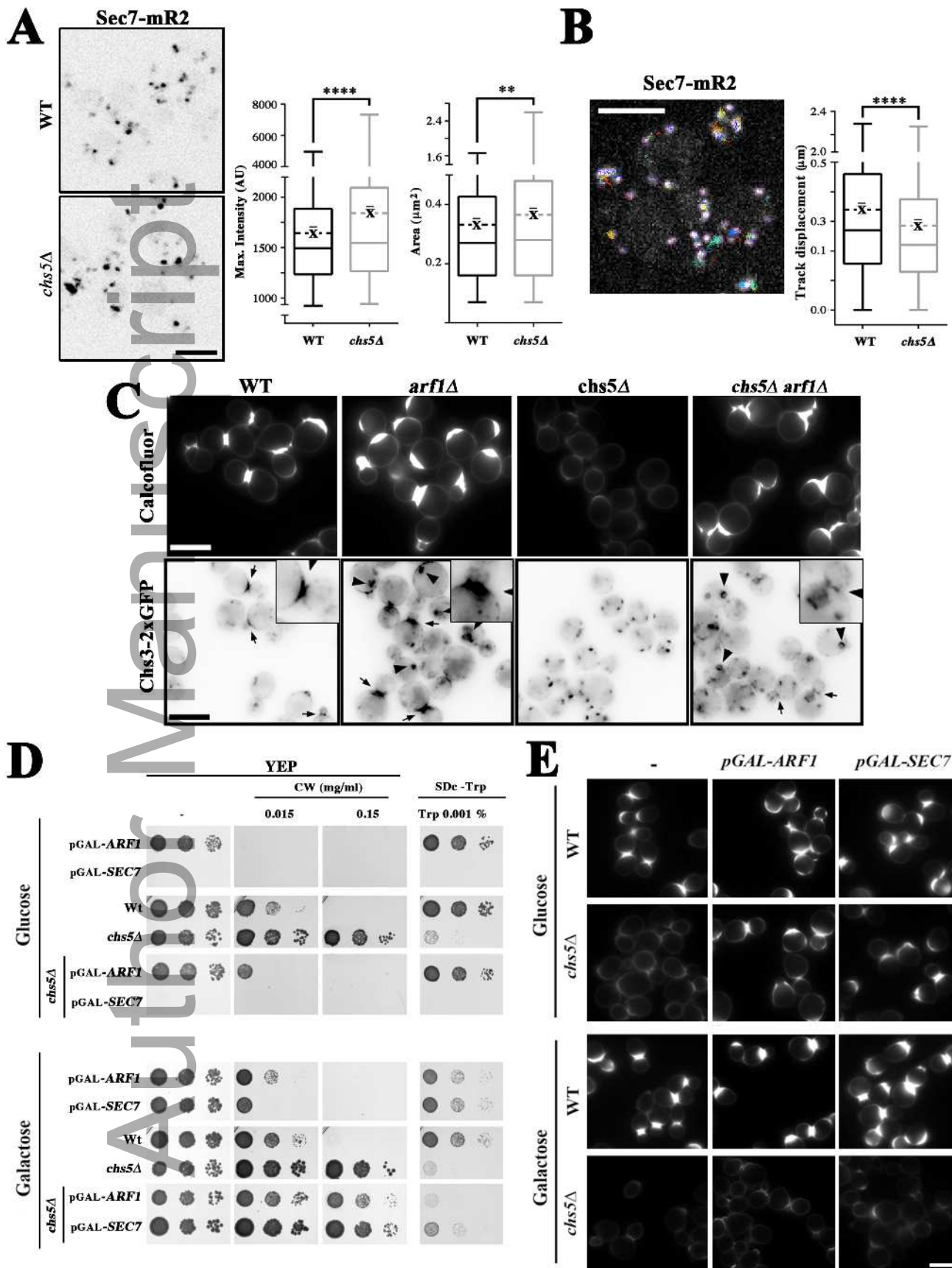
fsb2\_21615\_f2.tif

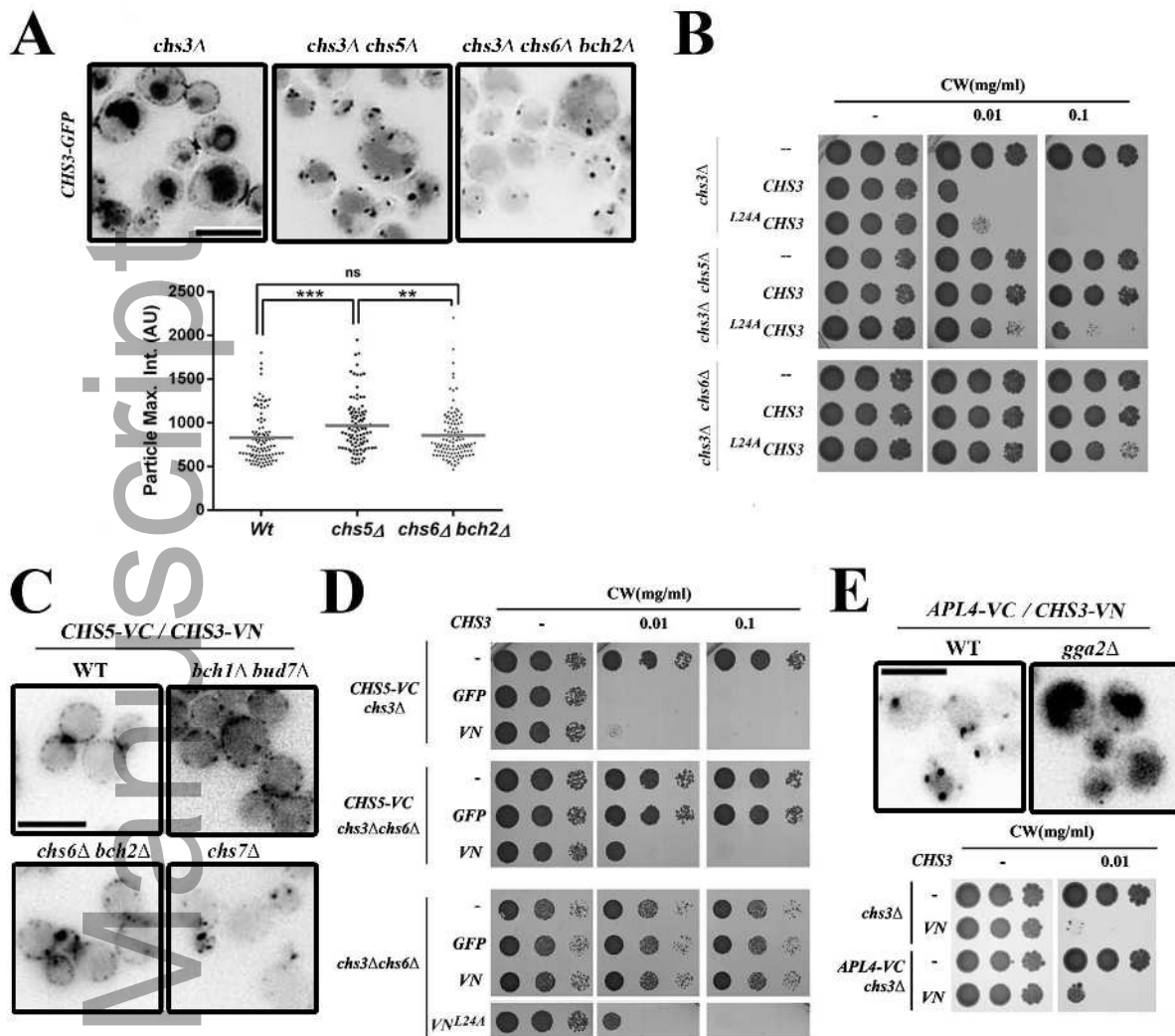


fsb2\_21615\_f3.tif

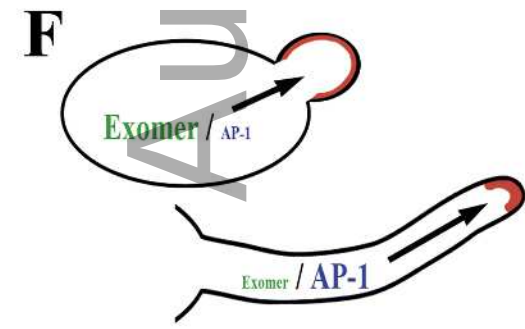
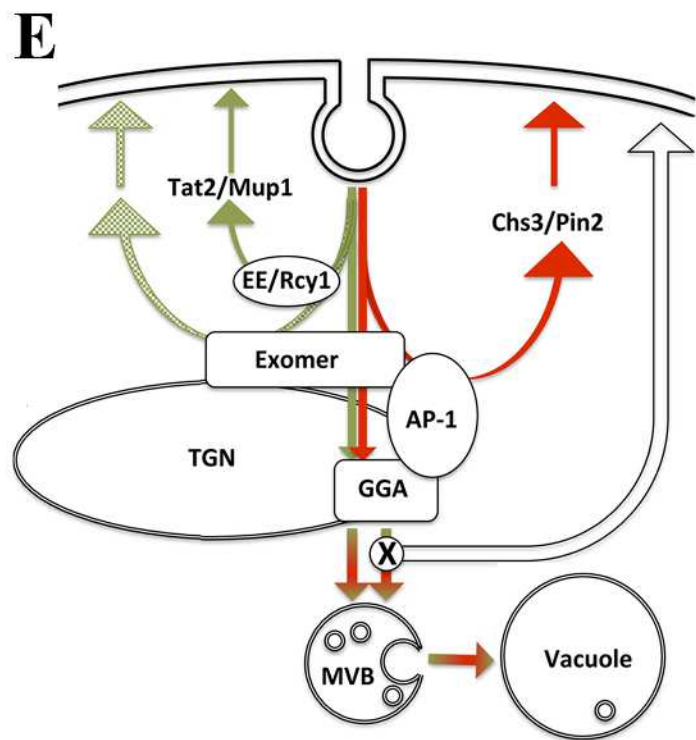
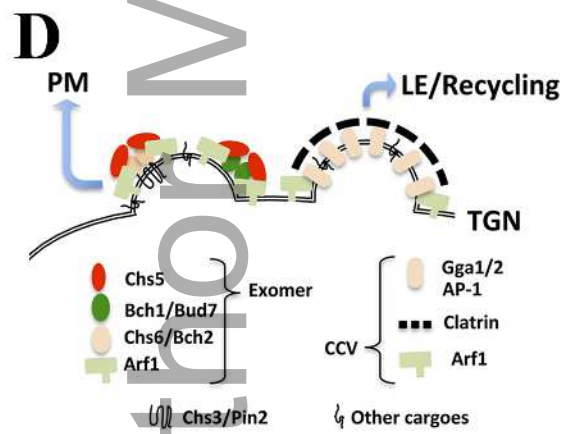
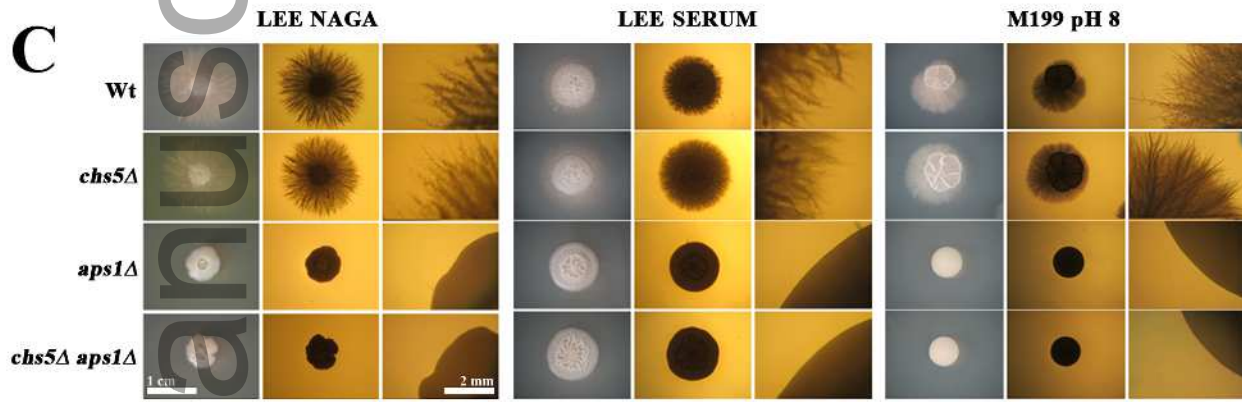
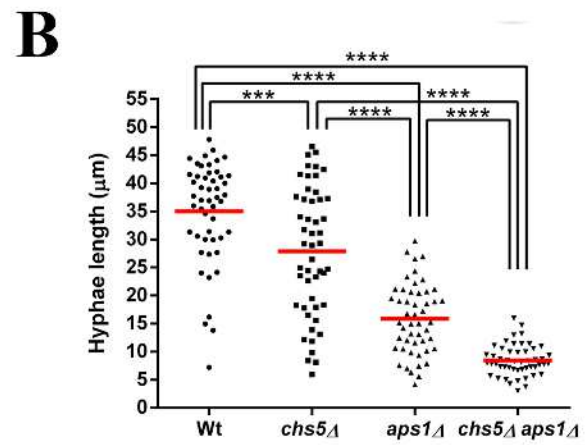
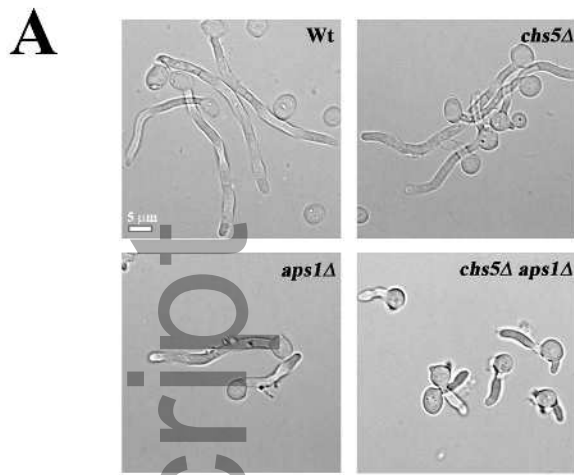


fsb2\_21615\_f4.tif





fsb2\_21615\_f6.tif



fsb2\_21615\_f7.tif